Novel catalysts in catalytic upcycling of common polymer wastes

Lijuan Deng[a], Wenshan Guo[a,b]*, Huu Hao Ngo[a,b,]*, Xinbo Zhang [b,c], Dong Wei[d], Qin Wei[e], Shihai Deng[f]

[a] Centre for Technology in Water and Wastewater, School of Civil and Environmental Engineering, University of Technology Sydney, NSW 2007, Australia

[b] Joint Research Centre for Protective Infrastructure Technology and Environmental Green Bioprocess, University of Technology Sydney and Tianjin Chengjian University

[c] Tianjin Key Laboratory of Aquatic Science and Technology, Tianjin Chengjian University, Jinjing Road 26, Tianjin 300384, China

[d] School of Water Conservancy and Environment, University of Jinan, Jinan, 250022, PR China

[e] Key Laboratory of Interfacial Reaction & Sensing Analysis in Universities of Shandong, School of Chemistry and Chemical Engineering, University of Jinan, Jinan, 250022, PR China

[f] School of Human Settlements and Civil Engineering, Xi'an Jiaotong University, Xi'an 710049, China

*Corresponding authors, Emails: wguo@uts.edu.au (W. Guo) and ngohuuhao121@gmail.com (H.H. Ngo)

Abstract

Catalytic upcycling is a promising waste management strategy that enhances the circularity of polymer wastes by transforming them into high-value-added products. This review presents the latest developments in novel catalysts, their applications and reaction mechanisms in upcycling approaches at various temperatures. High-temperature upcycling approaches include catalytic pyrolysis of polymers with biomass-derived biochar and carbonization with metal-based catalysts, which mainly produce hydrogen gas (H_2), mono-aromatic hydrocarbons and carbon nanomaterials. Electro-reforming, photo-reforming, glycolysis and enzyme-assisted depolymerisation take place in the low- and intermediate-temperature with metal-based catalysts, organo-catalysts and biocatalysts. Diverse value-added products are obtained from these approaches, such as terephthalic acid, formic acid, H_2, bis(2-hydroxyethyl) terephthalate, mono(2-hydroxyethyl) terephthalate, etc. The biomass-derived biochar has abundant functional groups, porous structure and large surface area that favour

the depolymerisation of polymer wastes. However, its catalytic activity declines after long-term reuse due to coke deposition and reduced essential components. Metal-based catalysts, on the other hand, have large amounts of active sites, ensure high electron transport capability, and encourage the generation of electron-hole pairs. However, they can suffer from formation of by-products, accumulation of organic intermediates, and declining activities during the separation process. Biocatalysts have surface regions (e.g., serine residue, tryptophan residue, amino acids) for effective hydrolysis of polymer wastes, but display limited thermostability and low activities at a wide pH range. To advance the field, future research should focus on developing novel catalysts with excellent thermostability and catalytic activities.

Keywords: Catalytic upcycling; Polymer wastes; Temperature; Catalysts; Biocatalysts

Abbreviations: BPA-PC, bisphenol A-based polycarbonate; BHET, bis(2-hydroxyethyl) terephthalate; *Bhr*PETase, A high-level secretory expression in *Bacillus subtilis* a PET hydrolase from the bacterium HR29; CB, conduction band; CNFs, carbon nanofibers; CNMs, carbon nanomaterials; CNTs, carbon nanotubes; EG, ethylene glycol; GA, glycolic aldehyde; GNSs, graphene nanosheets; HDPE, high-density polyethylene; *Is*PETase, *Ideonella sakaiensis* PETase; LCC, leaf-branch compost cutinase; LDPE, low-density polyethylene; MHET, mono(2-hydroxyethyl) terephthalate; MoPE, the selected amino acid sequence from the Antarctic bacterium *Moraxella* sp. TA144; Mt, million tonnes; PA, polyamide; PBAT, poly(butylene adipate-co-terephthalate); PBS, polybutylene succinate; PBSA, poly(butylene succinate-co-adipate); PC, polycarbonate; PCL, polycaprolactone; PE, polyethylene; PE-H, a novel carboxylic ester hydrolase identified in the genome of the marine hydrocarbonoclastic bacterium *Pseudomonas aestusnigri* VGXO14^{T}; PET, polyethylene terephthalate; PHAs, polyhydroxyalkanoates; PHB, polyhydroxybutyrate; PILs, protic ionic liquids; PLA, polylactic acid; PP, polypropylene; PP&A fibres, polyphthalamide fibres; PS, polystyrene; PUR, polyurethane; PVC, polyvinylchloride; TBD:MSA protic ionic salt, which formed by mixing equal moles of 1,5,7-triaza bicyclo[4.4.0]dec-5-ene (TBD) and methane sulfonic acid (MSA); TPA, terephthalic acid; VB, valence band; VPOM/CNNS hybrid, a novel Z-scheme heterojunction prepared by assembling highly-dispersed phosphovanadomolybdates ($H_5PMo_{12-n}V_nO_{40}$, VPOM) clusters onto the surface of graphitic carbon nitride nanosheets (g-C_3N_4 nanosheets, CNNS)

1. Introduction

Polymers are indispensable products of our life. The global usage of polymers will substantially increase from 460 million tonnes (Mt) in 2019 to 1231 Mt in 2060 [1] (Fig. 1). The most popular used plastic polymers include polyethylene (PE), polypropylene (PP), Polyphthalamide fibres (PP&A fibres), polyvinylchloride (PVC), polyethylene terephthalate (PET), polyurethane (PUR) and polystyrene (PS). PE accounts for the highest proportion of the global market (24-37%), followed by PP (16-21%), PP&A fibres (13-15%) and PVC (10-11.8%), while PET, PUR and PS cover 5-10.2%, 4-8.2%, and 5-7.6% of the global market share, respectively. Other types of polymers (e.g., polyester, polyamide (PA), polycarbonate (PC), polymethyl methacrylate, etc.) share up to 22% of the market. Due to the extensive use of polymers, the global polymer waste generation reached around 353 and 369 Mt in 2019 and 2021, respectively, which is estimated to considerably rise in the coming decades, reaching 1014 Mt in 2060 [2-4]. Current management methods dealing with polymer wastes are mainly landfills, incineration or combustion, recycling, and mismanagement (e.g., open burning, sea dumping, etc.). Landfills accounts for almost 50% of global polymer wastes, while the share of incineration remains at around 19%. However, only about 9% of the wastes is recycled worldwide. Moreover, the mismanaged wastes represent nearly 22% of polymer wastes [3].

Fig. 1.

Polymer wastes (especially micro- and nano-plastic particles) can cause serious environmental and human health issues: 1) changing global carbon cycle due to greenhouse gas emissions from waste degradation, and deteriorating the ocean carbon pump related carbon sequestration; 2) negatively changing the properties of soil and sediment (e.g., structure, composition, biodiversity, microbial activity, nutrient availability, etc.) due to the accumulation of plastic carbon in seabed sediments; 3) changing nutrient cycling by incorporating microplastics into marine particles; 4) adversely influencing marine organisms (e.g., starvation and drowning, altered gene and protein expression, declined reproductive ability and biodiversity, etc.) as waste-related microplastics, toxic chemicals, metals and pathogens can deteriorate water quality and disrupt marine food chains; and 5) posing potential risks to human health, causing nausea, headache, skin diseases, birth defect, diabetes, obesity, impaired immune function, cancer, etc. [2, 5-7]. Therefore, more efforts should be made to realise more effective waste management and enhance circularity of polymer wastes.

Recycling of polymer wastes is generally conducted at wide range of temperatures. The high-temperature (up to 15000 ºC, using plasma arc torches) recycling technologies (e.g.,

pyrolysis, conventional gasification, plasma gasification, etc.) convert the wastes to energy carriers (e.g., hydrogen, syngas). However, these technologies suffer from high investment and operating costs, as well as high energy and electricity demand. When the recycling technologies (e.g., hydrocracking, catalytic cracking) are operated at relatively low temperature (375-550 ºC), high yield of oil possessing properties similar to fossil fuels is obtained, along with decreased production cost, reduced energy requirement and shortened reaction time. Nevertheless, detailed pretreatment of the waste is required to eliminate impurities (e.g., chloride, nitrogen, organic materials) prior to recycling [8]. Upcycling is a new alternative to management of polymer wastes, which employs the wastes as feedstocks for synthesising high-value-added products (including new polymers, molecules or materials) [9, 10]. Five top plastic upcycling startups have been reported by StartUS Insights in recent years (2017-2019), including US-based startup CIRCULUS for producing high-quality plastic resins, UK-based startup CPE (Clean Planet Energy) for generating clean fuels and circular naphtha, Dutch startup VAN PLESTIK for making valuable products (e.g., chairs, tables, etc.) by a 3D printer, Portuguese startup SKIZO for textiles production, and US-based startup Closed Loop Plastics for an upcycled plastic monofilament for 3D printing [11].

Catalytic upcycling of polymers can be accomplished using different types of catalysts (e.g., metal-based catalysts, photocatalysts, biocatalysts, etc.). The catalysts play a key role in upcycling, which influence catalytic ability, conversion of polymer waste, selective formation, yield and purity of targeted products, and energy demand for the upcycling [9, 10]. Some review papers have discussed and examined the catalytic upcycling technologies in terms of their principles, mechanisms, advantages and challenges or opportunities [12-15]. Additionally, the complex relationship among polymers (especially polymeric chain structures), catalysts and catalytic reactions were demonstrated by [16]. Moreover, Wang et al. [17] presented the progress in development of nano-sized catalysts (nanocatalysts) for chemical upcycling of plastic wastes. Typical heterogeneous catalysts employed for catalytic upcycling of polymer wastes were highlights by Tan et al. [18]. However, these articles did not systematically discuss properties of different types of novel catalysts used in diverse upcycling approaches. In this perspective, this article aims to provide a comprehensive review on recent trends in developing novel catalysts and highlight the key role of four different types of catalysts (including biomass-derived biochar, metal-based catalysts, organo-catalysts and biocatalysts) in upcycling of polymers. It deeply discusses their applications in catalytic upcycling of polymers at different temperatures and corresponding mechanisms, as well as evaluates key characteristics of these catalysts.

2. Novel approaches and catalysts for high-temperature conversion of polymers

Catalytic pyrolysis and carbonization as high-temperature upcycling approaches can be used to depolymerise wide range of polymer wastes, such as high-density polyethylene (HDPE), low-density polyethylene (LDPE), PE, PP, PS, PVC, mixed plastics, etc. [19-21].

Comparison of different catalytic upcycling approaches using polymer wastes as feedstocks has been displayed in Table 1.

Table 1.

2.1. Catalytic pyrolysis

Catalytic pyrolysis proceeds at high temperature (e.g., 500-800 ºC) with novel biomass-derived biochar as acid catalyst which are recently applied in depolymerising polymers (e.g., corn stover-derived biochar [22, 23], nanocellulose-derived biochar [24], sewage sludge-derived biochar [25], corncob-derived biochar modified with Fe [26]). The catalyst pyrolysis, which is comprised of thermal decomposition, catalytic cracking (carbonium ion reaction) and upgrade over the biochar (Fig. 2), specifically explain the reaction mechanisms of polymer wastes on the novel biochar. Thermal decomposition of long-chain alkanes (i.e., LDPE) into small molecules is accomplished via free radical reaction mechanism consisting of chain initiation, chain propagation and chain termination in sequence. The chain initiation involves the formation of large amounts of small free radicals (e.g., $H^{\bullet}$, $CH_3^{\bullet}$, $C_xH_y^{\bullet}$) through thermal shock. The subsequent chain propagation undergoes three different reactions: 1) H-abstraction (H-transfer) between the existing radicals and hydrocarbon chains, leading to the formation of H_2, corresponding hydrocarbons (e.g., C_1-C_4) and new radicals (e.g., $C_{x1}H_{y1}^{\bullet}$); 2) β-scission reaction (splitting two carbons (C-C bond) away from the positively charged carbon atom by free radicals) which decomposes C-H bonds in the β-position by freeing electron of $C_mH_n^{\bullet}$ to form H_2, light hydrocarbon gas (e.g., CH_4, etc.), alkenes (olefins) and $H^{\bullet}$; 3) isomerisation reaction for breaking up C-C bonds in the β-position to form alkenes and new radicals (e.g., $C_{x2}H_{y2}^{\bullet}$). Final chain termination gives rise to the formation of H_2, CH_4, short-chain alkanes and alkenes by bonding of existing radicals [22, 24].

Fig. 2.

During catalytic cracking, carbonium ions are generated through abstracting hydrions from acid sites of the biochar by alkenes and subsequently adding the hydrions into C=C double linkages of the alkenes, or the formed carbonium ions reacting with alkanes. The isomerisation reaction takes place along with transforming the formed carbonium ions into more stable carbonium ions, followed by the β-scission of long-chain carbonium ions to generate alkenes and new carbonium ions, which go to next cycle or return hydrions back to the biochar to form alkenes [22, 24, 25]. Since the biochar contains acid sites and

dehydrogenation active sites, the alkenes generated from thermal decomposition and catalytic cracking can be further converted to aromatics and H_2 via the enhanced hydrogen transfer, cyclisation and Diels-Alder, and subsequent dehydrogenation and aromatisation [24, 25].

Biomass-derived biochar generally possesses relatively high specific surface area and acidity, porous structure, abundant functional groups (e.g., –C–OH, –C=C, –C=O and –C–H) and minerals (e.g., Ca, P, K, Fe, Mg, Mn, S, Cu, Zn, Na, Al, etc.), high hydrogen generation (up to 92 vol% in gas generated), high thermal stability, long-term cracking ability, and relatively long-term selectivity towards the generation of targeted products [23]. The inherent minerals (e.g., S, Fe, etc.) facilitate the acidity of biochar and selectivity by generating targeted products. The functional groups (e.g., P-OH, P=O, -C-O-P, -SO_3H, -COOH, -C-OH, etc.), minerals combined with oxygen (e.g., $AlPO_4$, CaO, etc.) and metal sulphides encourage the formation of diverse active sites (e.g., Lewis acid sites, Brønsted acid sites, dehydrogenation active sites, ring-opening active sites) on biochar. Consequently, hydrogen transfer, cyclisation, Diels-Alder, dehydrogenation and aromatisation are effectively prompted by these active sites, generating aromatics and H_2, while inhibiting the production of light hydrocarbons (such as CH_4, etc.). Moreover, the heavy aromatics can be further converted to lighter ones by hydrogenation and ring-opening reactions [22, 24, 25]. Besides, the inherent alkali and alkaline earth metallic species (AAEMs) also improve H_2 generation. The sp^2 hybridized orbitals of carbon enriched in the biochar framework could capture and separate charges from the inherent AAEMs (e.g., Na, K) in biochar, which further act as extra electron donors for reduction reaction of alkanes (e.g., low-density polyethylene (LDPE), waste disposable mask) for hydrogen generation [23, 24].

When disposing of disposable azo dyes-containing masks, corn stover-derived biochar could also adsorb dyes to generate clean oil, and maintain its adsorption ability towards dyes within 10 cycles [23]. Introducing metal species (e.g., Fe) into biochar enhances the biochar's surface acidity and increases acid sites, encouraging the formation of aromatics (especially mono-aromatics) and H_2 through various reactions (i.e., deoxygenation, rearrangement, polymerisation, cyclisation, H transfer, dehydrogenation, and aromatisation, etc.) [26]. The value-added products (e.g., aliphatic hydrocarbons, mono-aromatic hydrocarbons) generated using biochar can be used for producing jet and diesel fuels [22, 24; Table 2]. However, the used biochar without regeneration confronts with some challenges after a few cycles of reuse, such as certain damage of the porous structure [24, 25], declined H_2 yield due to the reduced functional species (e.g., Ca, K, Mg, etc.), the deposition of coke on the reused biochar [22, 23], and/or decreased active sites and catalytic activities of the reused biochar due to reduced contents of minerals and wax formation [24].

Table 2.

2.2. Carbonization

After pyrolysis, the obtained non-condensable hydrocarbon gases (C_xH_y) can be converted into carbon nanomaterials (CNMs) over metal-based catalysts through one type of carbonization methods, chemical vapor deposition [31]. This process is generally operated with high-temperature decomposition (e.g., 700-850 ºC) for generating H_2 and CNMs on the catalyst surface, comprising three steps: 1) pre-reduction (calcination): The catalysts are transformed into mixed oxide species (e.g., $LaNiO_x$, $NiCuO_x$, $FeMgO_x$, $MgMoO_x$, $FeMoO_x$, $CoMgO_x$, $CoMoO_x$, etc.), along with formation and rapid agglomeration of some non-interacted metal oxide species (e.g., NiO, Fe_2O_3, MoO_3, Co_3O_4, etc.). The mixed oxide species provide active sites for next two steps, enabling high catalytic growth activities in the final step; 2) reduction: The metal oxide species and mixed oxide species are reduced to highly dispersed metallic particles (e.g., Ni^0, Fe^0, Co^0, etc.), and metal alloy particles (e.g., Ni-Cu alloy, Fe-Mo alloy, etc.); 3) decomposition: This step transforms metal alloy particles to quasi-liquid state, and further elongates the metal alloy particles, as well as elongates or expands the mixed oxide species (e.g., $FeMgO_x$, $CoMgO_x$, etc.) in the quasi-liquid state to form metal and/or metallic carbide nanoparticles (e.g., Fe_3C, Mo_2C, $FeMoC_x$, Co_3C, $CoMoC_x$, etc.) along with H_2 generation in the presence of the hydrocarbon gases (C_xH_y). The highly dispersed metallic particles and the elongated metal alloy particles (e.g., Ni-Cu alloy particles) encourage the production of carbon nanofibers (CNFs) and/or carbon nanotubes (CNTs). The metal and/or metallic carbide particles (e.g., Fe_3C, $FeMoC_x$) not only prompt the growth of CNFs via tip growth mechanism, but also enhance the growth of graphene nanosheets (GNSs) [27-30].

Generally, the metal-based catalysts are transition 3d-metals catalysts, which have high surface area favourable for high decomposition and good catalytic activity due to the high dispersion and stable metal particle sites, facilitating aromatisation of hydrocarbon gases (e.g., CH_4, etc.) to form aromatic compounds for further growth of CNMs. Furthermore, the metal-based catalysts also have optimal composition (i.e., the optimal weight ratios of different metals in the catalysts, e.g., weight ratio of Fe/Mo in $FeMo_x$/MgO catalyst), which enable the conversion of all the components in the catalysts into corresponding mixed oxide species, metal oxides and metal alloy particles with quasi-liquid state nature, as well as the formation of optimal number of active sites for enhancing catalytic growth of CNMs. The CNMs obtained using the catalysts are highly crystalline and graphitized with high purity and thermal stability [27-30]. However, the metal-based catalysts cannot be regenerated and reused due to the changes in their composition after the process. Some recent review papers also summarized and discussed various carbonization methods (e.g., pressure carbonization, pyrolysis-gasification carbonization, active-template carbonization. etc.) with metal-based catalysts (e.g., Ni/Al_2O_3, $Ni/Mo/CaTiO_3$, $Fe/\gamma\text{-}Al_2O_3$, etc.) for production of CNMs (e.g., CNTs, CNFs, hollow carbon spheres, porous carbon, etc.) [20, 31, 32].

3. Novel approaches and catalysts for low- and intermediate-temperature depolymerisation of polymers

3.1. Electro-reforming

Electro-reforming is employed to limited types of polymers (e.g., HDPE, PP, PE, PET) [17-19, 33-35]. This upcycling approach using metal-based catalysts as electrodes has provided an opportunity for upcycling PET waste to value-added products. The electrolysis system can minimize plastic wastes, reduce energy demand by adopting thermodynamically favourable oxidation of PET hydrolysate and generating the target products (formate or formic acid), as well as avoid electrode corrosion by substantially inhibiting chlorine evolution reaction (CER) when proceeding in real seawater [34, 36].

Prior to electro-reforming, PET is pre-treated in alkaline solution, e.g., KOH at 60-80 ºC for 3-48 h, NaOH solution at 180 ºC for 2 h, to obtain PET hydrolysate, including terephthalic acid (TPA) or terephthalate and ethylene glycol (EG) (Eq. 1). After that, anodic EG oxidation under a strong alkaline environment (Eq. 2) and cathodic hydrogen evolution reaction (Eq. 3) occur as electro-reforming of PET hydrolysate. Glycolic aldehyde (GA) is initially generated by oxidization of EG, followed by three different pathways to generate formate or formic acid (Fig. 3): i) rapid oxidative C-C cleavage to formate; ii) The oxidization of GA to glycolic acid (minor intermediate), followed by slow C-C cleavage to formate; iii) The dehydrogenation of OH and C-H groups of GA to form glyoxal, further inducing C-C bond to form formic acid [35-37]. The occurrence of glycolic acid can result from glyoxal transformation in alkaline solution through Cannizzaro reaction [34].

Hydrolysis: $(PET)_n + (2n-1)H_2O \rightarrow nC_8H_6O_4$ (PTA) $+ nC_2H_6O_2$ (EG) (1)

Anode: $C_2H_6O_2 + 8OH^- \rightarrow 2HCOO^- + 6H_2O + 6e^-$ (2)

Cathode: $6H_2O + 6e^- \rightarrow 3H_2 + 6OH^-$ (3)

In addition, the CO_2 reduction reaction (CO_2RR) is also used as a cathodic reaction to produce the target product. Integrating oxidation of PET hydrolysate on the anode and CO_2RR on the cathode enables the production of formic acid from both electrodes (Eqs. (4) and (5)). The simultaneous generation of formic acid on two electrodes considerably increased Faradic efficiency, reaching 155% at cell voltage of 1.9 V [34].

Anode: $C_2H_6O_2 + 6OH^- \rightarrow 2HCOOH$ (formic acid) $+ 4H_2O + 6e^-$ (4)

Cathode: $CO_2 + 2H_2O + 2e^- \rightarrow HCOOH + 2OH^-$ (5)

Fig. 3.

The novel metal-based catalysts developed for electro-reforming process generally have large number of activate sites and superior intrinsic catalytic activity, exhibiting low interface charge transfer resistance and great electron transfer capability. They also demonstrate high stability and durability at high current (e.g., 100 mA, 200 mA) after several cycles (e.g., 5 cycles), and show excellent selectivity in terms of producing target products (> 80%) with high Faradic efficiency (> 85%) to ensure excellent electrochemical performance [34-37]. Moreover, 3D sponge-like Ni_3N/W_5N_4 Janus nanostructure provides high electrical conductivity (build-in electric field) at the heterointerface and resists the corrosion in chloride environment. Additionally, Ni_3N offers the appropriate sites for H* adsorption and further H_2 formation via hydrogen evolution reaction, while W_5N_4 provides the active sites (W 4d and O 2p) for H_2O adsorption to split H_2O molecule into H* and OH^- during the H_2O activation process [36]. However, some products will be formed due to the reconstruction of the catalysts during EG oxidation process, e.g., low crystalline metal oxy(hydroxide) analogue over $CoNi_{0.25}P$ [35]. Table 3 summarises the latest studies on low- and intermediate-temperature depolymerisation of polymer wastes using different types of catalysts.

Table 3.

3.2. Photo-reforming

Photo-reforming usually deals with diverse polymer wastes (LDPE, PE, PET, polylactic acid (PLA), PP, PS, PUR, PVC) [12, 15, 17-19, 33, 40, 42]. Prior to photo-reforming, the polymer wastes (e.g., PET, PLA) are generally pre-treated by alkaline solution to provoke the alkaline hydrolysis to generate monomers. Terephthalate can be isolated for further PET synthesis, while the subsequent photo-reforming process with metal-based photocatalysts at temperatures range of 20-40 ºC mainly involves the oxidation of monomers (mainly EG) and H_2 production through two pathways under visible-light irradiation (Fig. 4a). The first one is the exciting electrons move from photocatalyst's valence band (VB) to conduction band (CB), and reduce water to H_2. The photogenerated holes in photocatalyst's VB can oxidise organic substrate to smaller molecules. For instance, EG can be oxidised to glycolaldehyde, then further oxidised to glycolic acid and formic acid. Additionally, EG may also be converted to ethanol via hydrodeoxygenation. The other pathway involves organic substrate from plastic waste, which acts as an electron donor and is oxidised to smaller organic molecules. The photogenerated electrons then transfer from the photocatalyst to a cocatalyst and reduce water to H_2 [38-40]. When using the photocatalyst (e.g., Co-Ga_2O_3 nanosheets) to produce syngas from polymer wastes (e.g., PE bags, PP boxes and PET bottles) without alkaline pretreatment, H_2O could react with photogenerated electrons and holes and form H_2

and O_2 via light irradiation. After that, the •OH radicals released from H_2O and O_2 generated from previous step and/or O_2 from air took part in the degradation of polymer wastes [42]. For example, PE could be oxidised into CO_2 in photocatalyst's VB by utilising generated •OH radicals and O_2, meanwhile, O_2 was reduced to H_2O in the presence of the exciting electrons in the CB. Afterwards, CO_2 was reduced by ·COOH intermediates to CO in the CB, and H_2O was oxidised to O_2 in the VB (Fig. 4b).

Fig. 4.

The photo-reforming mechanism in the presence of photocatalyst with the bio-mimic Z-scheme heterostructure (e.g., VPOM/CNNS hybrid (a novel Z-scheme heterojunction prepared by assembling highly-dispersed phosphovanadomolybdates ($H_5PMo_{12-n}V_nO_{40}$, VPOM) clusters onto the surface of graphitic carbon nitride nanosheets (g-C_3N_4 nanosheets, CNNS)) is different (Fig. 4c). Using hybrid VPOM/CNNS photocatalyst with abundant surface-active sites (C and N elements in CNNS and O elements in VPOM as the main active sites) as an example, the Keggin structure and variable valence of vanadium atoms in phosphovanadomolybdates ($H_5PMo_{12-n}V_nO_{40}$, VPOM) promote the C–C bond cleavage reaction. As a semiconductor, graphitic carbon nitride nanosheets (CNNS) possesses a favourable band gap (~2.7 eV) and the conduction band potential to promote superoxide anion radical (O_2•$^-$) production. By assembling VPOM clusters onto the surface of CNNS through an electrostatic self-assembly strategy, the interface charge transport process can be realised in the VPOM/CNNS Z-scheme heterojunction (yellow band in Fig. 4c). Under illumination, photogenerated electrons from oxygen atom in the VB of VPOM cluster move to the CB in the transition metal (V or Mo) centres. Since the photogenerated holes in the CNNS are trapped by the VPOM via the Z-scheme mechanism, a Helmholtz double layer establishes in the VPOM/CNNS heterointerface. As a result, a build-in electric field is formed by negatively charged VPOM cluster and positively charged CNNS component, with the direction from CNNS to VPOM. This charge transfer bridge between electrons in the CB of VPOM and holes in the VB of CNNS facilitates the effective separation and transfer of photogenerated electrons flowing from VPOM to CNNS. After being trapped in the photogenerated holes of the CNNS, they transfer further from the VB to the CB of the CNNS, resulting in higher oxidative capacity. The highly reactive VPOM clusters accelerate the oxidative C-C bond cleavage in the polymer waste to form formaldehyde and carbon-cantered alkyl radical. The formaldehyde can be further oxidised to formic acid by O_2•$^-$ produced in the CB of the CNNS. On the other hand, long-chain alcohol can be converted from peroxide intermediate by the reaction of the alkyl radical with reactive oxygen species, which further contribute to the next C-C bond cleavage [41].

Metal-based catalysts in the photo-reforming have merits such as cost-effectiveness, allowing visible light adsorption, operation under alkaline conditions, easy separation from the solution after the process, high stability, short reaction time, increased number of electron-hole pairs through visible light irradiation due to the extensive light-responsive range, and higher H_2 generation activities [38-42]. Some unique properties of photocatalysts also improve the charge transfer and separation. For example, in carbonized polymer dots-graphitic carbon nitride composites (CPDs-CN), carbonized polymer dots (CPDs) acted as co-catalytic active sites and electron donors for enhancing charge separation, as well as broadened light-responsive range and redistributed electron-hole pairs, which increased electron densities in graphitic carbon nitride (GCN) [40]. Introducing Co atom into Ga_2O_3 nanosheets improved charge transfer due to greater density of states in the VB. Besides, the incorporation of Co atom could stabilise the intermediate products (•COOH and H^+) during the process with Co–Ga_2O_3 nanosheets as the photocatalyst by forming Co-Ga active sites and accumulating the charge of Co-H bond, which favoured the conversion of CO_2 to CO and H_2O as well as reduction of H_2O to H_2 [42]. Xing et al. [41] also concluded the VPOM/CNNS hybrid could enhance carrier transfer and separation at the interface of the heterojunction via Z-scheme transfer way.

The metal-based catalysts could also effectively oxidise most of hydrolysates (e.g., terephthalate, isophthalate, aliphatic components, etc.) generated from alkaline pre-treatment of PLA, PET and polyurethane (PUR). However, the aromatic components (e.g., 2,6-diaminotoluene) generated by alkaline hydrolysis of PUR are recalcitrant to photo-oxidation. The total conversion of polymer wastes is not high (e.g., < 40% for PLA, PET and PUR using CdS/CdO_x as the photocatalyst) due to the incomplete mineralisation of the wastes to CO_2. The accumulation of organic intermediates reduces H_2 production. The separation or drying process for reusing photocatalysts might cause agglomeration and further deteriorate the activity of photocatalysts [38, 39].

3.3. Glycolysis

Targeted feedstocks for glycolysis generally include bisphenol A-based polycarbonate (BPA-PC), PET and PUR [17, 46, 49, 63]. Glycolysis of PET generally occurs in the presence of EG at temperatures ranging from 160 to 300 ºC, which is divided into metal-based and metal-free glycolysis. The commonly used mental-based catalysts include iron oxide, cobalt oxide, and manganese oxide [43, 44, 64]. When employing metal-based carbon nano-catalyst, glycolysis is accomplished via the following mechanism (Fig. 5a): 1) the hydrogen bonding interaction between the EG molecules can be enhanced through dispersing metal-based carbon nano-catalyst in EG; 2) metal cations (e.g., cations of magnetite, Fe^{2+} or Fe^{3+}) interact with the carbonyl's oxygen of PET, thereby partially increasing the positive charge of the carbonyl group. At the same time, the interaction between carbon nano-catalyst

and EG creates a lengthened hydroxyl O–H bond and more electronegative EG oxygen atom; 3) The nucleophile oxygen of EG attacks carbon atom of the PET's carbonyl group, establishing a new C–O bond, while the PET's acyl-oxygen bond is broken down. The reaction occurs in a repeated manner to produce monomer (e.g., bis(2-hydroxyethyl) terephthalate, BHET).

Fig. 5

Protic ionic liquids (PILs) have provided good opportunities for PET glycolysis. When using PIL as the organo-catalyst for glycolysis of PET, the oxygen atom in anion of PIL initially interacts with hydrogen of hydroxyl on EG (proton abstraction), which enables the formation of H-bond and glycol anion (nucleophilic species). Additionally, the protonated cation of PIL can also activate the carbonyl of PET. After that, the carbonyl carbon of PET is attacked by the oxygen atom of glycol anion to break down the PET chain and further generate intermediates. Different compositions of PILs can be obtained by mixing 1,5-diazabicyclo [4.3.0] -5-nonene (DBN) with phenol or phenol derivatives. For example, when mixing DBN and 4-methylphenol and making PIL(p-cresol) as the catalyst (made from), glycol anion was bonded with intermediate 1 (Int. 1, Fig. 5b), along with transferring of hydrogen atom of N-H in cation of PIL to the oxygen atom in intermediate 2 (Int. 2, Fig. 5b) [49].

Jehanno et al. [51, 52] also reported glycolysis of BPA-PC (Bisphenol A-based polycarbonate) and PET using TBD:MSA protic ionic salt, which formed by mixing equal moles of 1,5,7-triaza bicyclo[4.4.0]dec-5-ene (TBD) and methane sulfonic acid (MSA). The anion of TBD:MSA protonated the hydroxyl-methyl moiety of the intermediate 3 (Int. 3, Fig. 5b). These steps lead to the formation of oligomers, then dimers and finally BHET monomer. Glycolysis of bisphenol A-based polycarbonate (BPA-PC) by TBD:MSA consists of two steps, in which the first step is similar with glycolysis of PET. The second step involves the proton transfer from the second hydrogen of hydroxyl on EG to a molecular of BPA (the leaving group), followed by the formation of a second molecule of BPA and cyclic ethylene carbonate through ring-closure of EG.

During glycolysis process, the metal-based catalysts exhibit special polarity and high surface area, good catalytic activity (up to 100% of BHET yield), high selectivity towards BHET generation (> 80%), thermal stability, recyclability, and easy magnetic recoverability [44-46]. Nabid et al. [45] developed a magnetic bifunctional catalyst by coating Fe_3O_4 nanoparticles on boron nitride nanosheets (Fe_3O_4 NPs@h-BNNS), which could prompt more efficient glycolysis of PET due to π-π interaction between aromatic PET and h-BNNS. The co-existence of boron atoms (acidic sites) and nitrogen atoms (basic sites) can enhance

electrophilic properties of carbonyl groups in PET and abstract hydrogen from hydroxyl groups, respectively, thereby improving the EG's nucleophilic attack on PET. The presence of halometallate-based ionic liquids shell in magnetic nanocatalyst Fe_3O_4@SiO_2@(mim)[$FeCl_4$] (mim: methylimidazolium) positively affected the PET glycolysis via the pathway similar with that for PIL. At 180 °C, it could be recovered magnetically and reused for up to 12 cycles with minimum loss in the catalytic activity, achieving 84% BHET yield [46].

The organo-catalysts have high thermal stability and high recycling ability (e.g., ≥ 7 times without considerable decline in the activity), as well as enable 92% of BHET and 89% of BPA yield during glycolysis of PET and BPA-PC, respectively [50-53]. The presence of electron donating group and its position of benzene ring in PIL are also of importance in catalytic performance. For example, anion with electron donating group (-CH_3) in the ortho or para positions of the benzene ring in PIL enhanced the interaction of the catalysts with EG by increasing electron cloud density of phenoxy ion [49]. The proton transfer favoured the regeneration of PIL catalyst, which was accomplished by transferring hydrogen in oxygen atom of glycol anion to nitrogen atom of PIL cation (Fig. 5(b); Wang et al. [49]). However, by-products could be formed (e.g., dimer, oligomers, EG-derived chemicals attached with a bis-carbonate of BPA) when using PIL for glycolysis of PET due to chemical equilibrium between dimer and BHET monomer [49, 50]. Other causes include the formation of linear carbonate through non-cyclization after the nucleophilic attack of EG or ring-opening of the formed cyclic carbonate by BPA generated during glycolysis of BPA-PC [51].

3.4. Enzyme-assisted depolymerisation

A new developed technology for plastic upcycling is enzymatic depolymerisation. Esterolytic enzymes, such as esterases, cutinases and lipases, have been used for decomposing PA, poly(butylene adipate-co-terephthalate) (PBAT), polybutylene succinate (PBS), poly(butylene succinate-co-adipate) (PBSA), polycaprolactone (PCL), PET, polyhydroxyalkanoates (PHAs), polyhydroxybutyrate (PHB), PLA, and PUR [12, 65-67]. The PET-degrading enzyme *Ideonella sakaiensis* PETase is a cutinase-like enzyme [54]. PET depolymerisation using the PETase enzyme at low temperatures (e.g., 30-72 ºC) includes deprotonation of the catalytic serine by the catalytic histidine residue from the catalytic triad to form a nucleophilic alkoxide group, nucleophilic attack by the deprotonated catalytic serine on the carbonyl carbon of PET to break down acyl-oxygen bond of PET, and final generation of mono(2-hydroxyethyl) terephthalate (MHET), TPA and/or BHET [56, 58, 61]. After BHET is cleaved to MHET and EG by the PETase enzyme, the further MHET hydrolysis using MHETase can be accomplished by a two-step serine hydrolase mechanism considering the triad constructed by catalytic residues His528, Asp492 and nucleophile Ser225. The first step involves the release of an acyl-enzyme intermediate (AEI) and EG via

acylation, in which His528 deprotonated the catalytic serine (Ser225) to stimulate nucleophilic attack of Ser225 on the carbonyl carbon of MHET and further form C-O bond between carbonyl carbon of MHET and Ser225, along with breaking C-O ester bond of MHET and liberating EG from the active site. The second step generates TPA by nucleophilic attack of one water molecule on the AEI via diacylation, forming C-O bond between MHET and the water molecule while breaking C-O bond of AEI [61].

Biocatalysts originated from bacteria strains, isolated from soil or marine samples possess unique structure features associated with polymer depolymerisation. Generally, to achieve efficient PET hydrolysis, PET-hydrolysing enzyme based on *Ideonella sakaiensis* (*Is*PETase) should have properties as follows: 1) a classical α/β hydrolase core domain with/without a lid domain enclosing active site, which usually contains a wide-open active site cleft easily accessed by polymer substrates; 2) surface regions containing serine residue, tryptophan residue and amino acids with extended loop region (β8-α6) to enhance polarised surface charge, enzyme activity and substrate binding; and/or 3) an additional disulphide bond to stabilise the extensive loop and/or the lid domain [56, 57, 59, 61, 66]. Sagong et al. [66] studied anther similar PET hydrolase from *Rhizobacter gummiphilus* (*Rg*PETase). *Rg*PETase exhibited an even conformation of wobbling tryptophan containing loop (WW-loop), stabilised by interactions between the loop and its adjacent regions. Negative surface charge of the WW-loop favoured PET degradation. Nikolaivits et al. [54] developed a recombinant enzyme (MoPE) from Antarctic bacterium *Moraxella sp.* with the catalytic triad containing residues Ser189, Asp234 and His264. Compared with confirmed PET-hydrolases, MoPE shows 42–46% identity and has psychrophilic hydrolases characteristics. Moreover, MoPE has three disulphide bonds, of which the unique one connects its N-terminal loop. Despite being obtained under cold condition, the high activity of MoPE could maintain at relatively high temperature (e.g., retaining > 80% of the maximum activity at 20-35 ºC). In another study, Xi et al. [55] reported a PET degrading enzyme from *Bacillus subtilis* strain (*Bhr*PETase), which showed high PET hydrolysing activity when comparing with cutinase and *Is*PETase enzymes. Although *Bhr*PETase with the catalytic triad constituted by residues Ser165, Asp210, and His242 showed 94% identity with the leaf-branch compost cutinase, it was proved to be a more thermostable enzyme with melting temperature of 101 ºC than that of the cutinase (90 ºC).

The biocatalysts also demonstrate high potential in degrading wide range of polymer wastes. Apart from effective PET hydrolysis (Table 3), MoPE exhibited certain ability in degrading other polymers by end scission or random scission of polymer chain, e.g., polycaprolactone (PCL, weight loss of 33.4%), polyhydroxy butyrate (PHB, 8.9%), polybutylene succinate (PBS, 5.3%), polyurethane (PUR, 3.9%) [54]. Some enzymes identified from waste degrading facility or microbial community show highly hydrolysing activity for PLA, e.g., MGS0156 with highly hydrophobic active site (catalytic residues Ser232, His373, and Asp350) and GEN0105 (catalytic triad consisting of residues Ser168, His292 and Glu262) involving effectively depolymerisation of solid PLA via endo- and exo-

esterase cleavage (degrading > 70% of solid PLA overnight) [56]. Nevertheless, the activity of the biocatalyst may be only kept at narrow pH range (e.g., pH of 6-8 for *Bhr*PETase) and can be deteriorated at higher temperature (e.g., 90% loss of activity after 2 h at 50 ºC for MoPE, degradation products of 6.3 mM at 70 ºC vs 4.95 mM at 80 ºC for *Bhr*PETase) [54, 55].

The PET-hydrolysing activity of biocatalyst can be improved by site directed mutagenesis, mutation of active site residues or identifying stabilising mutations based on structure-based machine learning algorithm (e.g., three-dimensional self-supervised convolutional neural network). Table 3 indicates that the newly developed PETase variants not only display great depolymerisation level, but also induce the generation of more PET monomers compared with the original enzymes as well as have the high potential in depolymerising real-world PET plastics. PE-H was identified in the genome of the marine hydrocarbonoclastic bacterium *Pseudomonas aestusnigri*. After introducing a single amino acid substitution (Y250S) into PE-H to replace the aromatic residue tyrosine adjacent to the active site histidine, the obtained variant PE-H (Y250S) showed the enhanced enzymatical activity towards larger substrates (e.g., PET film from a commercial PET bottle (PETb)) compared with PE-H. This was due to the increase in cavity volume of active site with catalytic triad (residues Ser171, Asp217 and His249) through a stabilised loop arrangement between the hydroxyl group of Y250 and the backbone amine of E102, which limited the active site cleft [57]. The leaf-branch compost cutinase (LCC) variants obtained through subjecting some amino acid residues of LCC to site-specific saturation mutations contained the active sites with the catalytic residues (Ser165, Asp210 and His242) and exhibited higher specific activity (up to 34% improvement) than wide-type LCC [58]. Introducing double mutation (DM) of serine and isoleucine residues to biocatalysts considerably elevated their activities (e.g., by 3~10 times) (Table 3; Chen et al. [59]). Compared to *Is*PETase, the two *Is*PETase variants (ThermoPETase and DuraPETase) showed higher thermostability (increasing melting temperature by 8.8-31 ºC). Moreover, DuraPETase demonstrated considerably greater PET degradation ability for long-term operation (300-fold increment at 37 ºC for 10 days) [67, 68]. According to a structure-based machine learning algorithm, the functional, active, stable and tolerant PETase (FAST-PETase) including three predicated mutations and two ThermoPETase scaffolds with catalytic triad (Ser160, Asp206 and His237) possessed significantly higher activity (2.4-38 times higher) at 40-50 ºC than ThermoPETase alone, along with excellent PET-hydrolysing activity at 50 ºC (Table 3). Its potential in hydrolysing PET under mild temperatures (30-40 ºC) and moderate pH conditions (6.5-8.0) noticeably enhanced (up to ~38 mM of PET monomers released) compared to wide-type PETase, ThermoPETase, DuraPETase, and LCC (up to ~14 mM of PET monomers released with each one) [60]. It must be pointed out that the increased temperature (e.g.., > 60 ºC) induced the decline in the DM-mediated enhancement in the activity (e.g., LCC-DM) [59]. The thermostability of biocatalysts could be enhanced by employing a disulphide bridge to replace the divalent-metal binding sites which consist of side chains of three acidic amino acid residues. This method allowed the production of a

thermostable LCC variant with higher melting temperature (94.5 ºC; increasing by 9.8 ºC compared with the wide-type LCC). After adding high-activity mutations and other thermostable mutations to this thermostable variant, the newly formed variants possessed higher melting temperatures (+ 9.3 ºC ~ + 13.4 ºC) than wide-type LCC. One of these new variants could depolymerise around 90% of PET to monomers over 10 h at high temperature of 72 ºC (Table 3; Tournier et al. [58]).

As the intermediate products of PET hydrolysis (e.g., MHET, BHET) inhibit polyester hydrolase, the two-enzyme system has been developed to improve the degradation of the intermediate products using a second enzyme. Immobilized *Tf*Ca was obtained by immobilizing the carboxylesterase *Tf*Ca variant from *Thermobifida fusca* KW3 on SulfoLink resin. When employing both the metagenome-derived LCC and immobilised *Tf*Ca for PET hydrolysis, the immobilised *Tf*Ca effectively hydrolysed MHET and BHET, resulting in TPA as the main products [69]. To selectively and complete convert MHET, a novel MHETase was identified. The core domain of MHETase was similar with that of PETase (especially ferulic acid esterase), which had an extensive lid domain covering part of active sites with catalytic triad (Ser225, Asp492, and His528) and holding a well-coordinated Ca^{2+} cation for stabilising the enzyme. Compared to PETase, it had a highly acidic surface charge and five disulphide bonds, of which one at the active site was bonded with cysteines in the vicinity of the catalytic residues. Adding MHETase into the two-enzyme system (*Is*PETase/MHETase system) could significantly improve the depolymerisation at 30 ºC to generate TPA as the only product, even with very low concentration of MHETase (e.g., 0.1 mgMHETase/gPET) relative to PETase (e.g., 2 mg PETase/gPET) [61]. MoPE combined with FoFaeC (a feruloyl esterase) could convert PET film or powder to TPA as the only final product (Table 3; Nikolaivits et al. [54]). The combined hydrolases (e.g., mixture of esterase and amidase) were also found to enable the effective hydrolysis of polymer wastes (e.g., thermoplastic polyurethanes (TPU)) through degrading macromolecules and releasing low molar mass molecules with urethane bond by the esterase, which were further hydrolysed by the amidase. However, the final product contained a potential inhibitor with a urethane bond for the activity of the biocatalyst [62].

4. Social significance

This article provides fundamental information about the negative effects of the polymer wastes on environment and human health, and current recycling technologies. Additionally, it clarifies the mechanisms about six different catalytic upcycling approaches, as well as deeply and systematically discusses the approaches and the novel catalysts employed. Hence, this review offers useful and valuable information to a broad audience, including academic researchers and scientists, waste management or disposal industries and public:

i) Academic researchers and scientists can obtain the latest knowledge about upcycling approaches and the development of highly stable and active catalysts to increase their scalability.

ii) The knowledge about the catalytic upcycling of polymer wastes can not only be adopted by waste management or disposal industries for training purposes, but also modify or upgrade their current waste disposal systems, or take initiatives in replacing the processes by the novel upcycling strategies.

iii) Currently, public awareness on waste segregation/separation and management varies in different regions. According to a recent survey in Europe, large number of respondents (> 20%) have yet to recognise the adverse impacts of plastic waste on soil, air and climate change. Around 74% of respondents do the segregation of plastic waste and proper disposal. Nevertheless, some of them (6%) do not sort the waste [70]. As reported by Wang et al. [71], there is no link between public's recycling knowledge and their attitudes toward recycling of household solid waste (behaviour and willingness to take part in the recycling) in urban areas of China. Therefore, it is need for conducting education to increase public awareness about plastic waste management and improve the attitudes (behaviour and willingness) toward better polymer waste management. Thus, this review gives the public some ideas about current polymer waste generation, main types of polymer wastes, and current management methods. This review also provides an in-depth knowledge of the sustainable alternative to upcycle polymer waste and produce value-added products.

5. Future research perspectives

High-temperature conversion approaches are subjected to high energy demand and operational costs. Both biomass-derived biochar and metal-based catalysts can be used in these conversion approaches. Biomass-derived biochar is generally prepared via microwave-assisted pyrolysis process [22-24, 26]. The stable metal-based catalysts are obtained by calcinating in an atmosphere at high temperatures (500-800 ºC) [27-30]. After a few cycles of reuse, the catalytic activities and active sites decline on the used biochar due to the deposition of coke on the biochar, decreased contents of minerals and wax formation. The metal-based catalysts for growth of CNMs can only be used once as the conversion process changes their compositions. Current studies about low- and intermediate-temperature conversion of polymer wastes mainly concentrate on electro-reforming, photo-reforming, glycolysis and enzyme-assisted depolymerisation. Metal-based catalysts can result in the formation of by-products, the accumulation of organic intermediates, and deteriorated activity. For organo-catalysts, by-products (e.g., dimer, oligomers, etc.) can be formed during glycolysis. Biocatalysts also face some problems, such as declined activity at wide pH range, unsatisfactory thermostability, low catalytic activity for degrading intermediate products

(e.g., MHET, BHET, etc.), and the presence of potential inhibitor in the final product. Therefore, future research priorities are specified as follows:

1) More types of catalysts for high-temperature conversion strategies are needed. The newly developed catalysts can be employed at relatively lower temperature (e.g., 300-500 ºC) to save energy and cost. Additionally, the novel catalysts should have the ability to moderate the deposition of coke and wax formation, as well as maintain their porous structures and essential components for long-term reuse.
2) It requires to improve the properties of metal-based catalysts for low-temperature conversion processes. The new catalysts should enhance selective conversion of polymer wastes into targeted products and minimize the accumulation of intermediate products. Moreover, it is vital to develop advanced separation methods for reusing catalysts as well as maintain activities of the catalysts.
3) New organo-catalysts are required to be synthesized to inhibit the formation of by-products.
4) Novel biocatalysts should have greater catalytic activity at wider pH range, higher thermostability, higher potential in degrading intermediate products, and catalytic activities.
5) More studies should focus on novel hydrolases for two-enzyme system to prompt effective hydrolysis of polymer wastes, while limiting the accumulation of intermediate products and the formation of inhibitors in final products.
6) More time-saving, cost-effective and environmentally friendly purification methods after upcycling need to be developed to obtain targeted products with high purity.
7) Education program should be established to increase the public awareness towards the environmental pollution of polymer wastes, as well as encourage younger people and those with higher education to proactively take part in upcycling of polymer wastes and look for more routes to deal with the wastes.

6. Conclusions

This review highlights the latest developments in novel catalysts for catalytic upcycling of polymer waste and corresponding upcycling approaches at different temperatures. High-temperature conversion methods include catalytic pyrolysis and carbonization at 500-800°C. Biomass-derived biochar and transition 3d-metals catalysts facilitate the formation of H_2, aromatics, and/or CNMs due to their abundant functional groups, large surface area, and high catalytic activity. However, the reusability of biochar is compromised by the deposition of coke on the biochar, wax formation, and a decline in essential component content. Low- and intermediate-temperature conversion processes such as electro-reforming, photo-reforming, glycolysis, and enzyme-assisted depolymerization are operated at 20-225°C. Metal-based catalysts offer many active sites, enhance electron transport and generation of electron-hole

668 pairs, and improve selectivity in producing targeted products and charge transfer and
669 separation. However, the reconstruction of the catalysts during the depolymerization process
670 can induce the formation of some products, and their activity is reduced by the separation or
671 drying process for reuse. Organo-catalysts lead to the formation of by-products (e.g., dimer,
672 oligomers, etc.) despite a high yield of targeted products. Biocatalysts have a classical
673 hydrolase core domain, surface regions, and/or an additional disulfide for efficient hydrolysis
674 of polymer waste. Nevertheless, they suffer from decreased activity at a wide pH range and
675 low thermostability. A broad audience, including academic researchers and scientists, waste
676 management or disposal industries and the public, can get useful knowledge and information
677 regarding commonly generated polymer wastes and their upcycling approaches to advance
678 related research and practices, upgrade the current waste management systems, and improve
679 public awareness on plastic waste management. Future research should focus on developing
680 novel catalysts with improved thermostability, highly selective conversion of polymer waste
681 into targeted products, and limited accumulation of intermediate products.

682

683 **Acknowledgement**

684 This research was supported by University of Technology Sydney, Australia (UTS,
685 RIA- NGO, UTS SRS-NGO and UTS SRS-GUO)

686

687

688 **References**

689 [dataset] [1] OECD, Plastics use by polymer-projections, Global Plastics Outlook Database,
690 2022
691 https://stats.oecd.org/viewhtml.aspx?datasetcode=PLASTIC_USE_V2_2&lang=en
692 (Accessed 11 January 2023).

693 [2] S.S. Ali, T. Elsamahy, E. Koutra, M. Kornaros, M. El-Sheekh, E.A. Abdelkarim, D.
694 Zhu, J. Sun, Degradation of conventional plastic wastes in the environment: A review
695 on current status of knowledge and future perspectives of disposal, Sci. Total Environ.
696 771 (2021) 144719. https://doi.org/10.1016/j.scitotenv.2020.144719

697 [3] OECD, Global Plastics Outlook: Policy Scenarios to 2060. OECD Publishing, Paris.
698 https://doi.org/10.1787/aa1edf33-en, 2022 (Accessed 11 January 2023).

699 [4] C. Wang, Y. Liu, W.Q. Chen, B. Zhu, S. Qu, M. Xu, Critical review of global plastics
700 stock and flow data, J Ind. Ecol. 25 (2021) 1300-1317.
701 https://doi.org/10.1111/jiec.13125

702 [5] Q. Chen, A. Allgeier, D. Yin, H. Hollert, Leaching of endocrine disrupting chemicals
703 from marine microplastics and mesoplastics under common life stress conditions,
704 Environ. Int. 130 (2019) 104938. https://doi.org/10.1016/j.envint.2019.104938

705 [6] M. MacLeod, H.P.H. Arp, M.B. Tekman, A. Jahnke, The global threat from plastic
706 pollution, Science 373 (2021) 61–65. https://doi.org/10.1126/science.abg5433

707 [7] UNEP, From pollution to solution: A global assessment of marine litter and plastic
708 pollution. Synthesis. Nairobi (ISBN: 978-92-807-3881-0).
709 https://wedocs.unep.org/bitstream/handle/20.500.11822/36965/POLSOLSum.pdf,
710 2021. (Accessed 11 January 2023)

711 [8] M. Solis, S. Silveira, Technologies for chemical recycling of household plastics – A
712 technical review and TRL assessment, Waste Manage. 105 (2020) 128–138.
713 https://doi.org/10.1016/j.wasman.2020.01.038

714 [9] M. Chu, Y. Liu, X. Lou, Q. Zhang, J. Chen, Rational Design of Chemical Catalysis for
715 Plastic Recycling, ACS Catal. 12 (2022) 4659−4679.
716 https://doi.org/10.1021/acscatal.2c01286

717 [10] C. Jehanno, J.W. Alty, M. Roosen, S. De Meester, A.P. Dove, E.Y.X. Chen, F.A.
718 Leibfarth, H. Sardon, Critical advances and future opportunities in upcycling
719 commodity polymers, Nature 603 (2022) 803–814. https://doi.org/10.1038/s41586-021-
720 04350-0

[11] StartUS Insights, 5 Top Plastic Upcycling Startups. https://www.startus-insights.com/innovators-guide/plastic-upcycling-startups/ (Accessed 11 January 2023)

[12] H. Zhou, Y. Wang, Y. Ren, Z. Li, X. Kong, M. Shao, H. Duan, Plastic Waste Valorization by Leveraging Multidisciplinary Catalytic Technologies, ACS Catal. 12 (2022) 9307-9324. https://doi.org/10.1021/acscatal.2c02775

[13] M.-Q. Zhang, M. Wang, B. Sun, C. Hu, D. Xiao, D. Ma, Catalytic strategies for upvaluing plastic wastes, Chem 8 (2022) 2912-2923. https://doi.org/10.1016/j.chempr.2022.08.004

[14] S.C. Kosloski-Oh, Z.A. Wood, Y. Manjarrez, J.P. de los Rios, M. Fieser, Catalytic methods for chemical recycling or upcycling of commercial polymers, Mater. Horiz. 8 (2021) 1084-1129. https://doi.org/10.1039/D0MH01286F

[15] X. Chen, Y. Wang, L. Zhang, Recent Progresses in the Chemical Upcycling of Plastic Wastes, ChemSusChem 14 (2021) 4137-4151. https://doi.org/10.1002/cssc.202100868

[16] M. Chu, Y. Liu, X. Lou, Q. Zhang, J. Chen, Rational Design of Chemical Catalysis for Plastic Recycling, ACS Catal. 12 (2022) 4659-4679. https://doi.org/10.1021/acscatal.2c01286

[17] C. Wang, H. Han, Y. Wu, D. Astruc, Nanocatalyzed upcycling of the plastic wastes for a circular economy, Coord. Chem. Rev. 458 (2022) 214422. https://doi.org/10.1016/j.ccr.2022.214422

[18] T. Tan, W. Wang, K. Zhang, Z. Zhan, W. Deng, Q. Zhang, Y. Wang, Upcycling Plastic Wastes into Value-Added Products by Heterogeneous Catalysis, ChemSusChem 15 (2022) e202200522. https://doi.org/10.1002/cssc.202200522

[19] R. Balu, N.K. Dutta, N. Roy Choudhury, Plastic Waste Upcycling: A Sustainable Solution for Waste Management, Product Development, and Circular Economy. Polymers 14 (2022) 4788. https://doi.org/10.3390/polym14224788

[20] L. Dai, O. Karakas, Y. Cheng, K. Cobb, P. Chen, R. Ruan, A review on carbon materials production from plastic wastes, Chem. Eng. J. 453 (2023) 139725. https://doi.org/10.1016/j.cej.2022.139725

[21] S. Pourebrahimi, Upcycling face mask wastes generated during COVID-19 into value-added engineering materials: A review, Sci. Total Environ. 851 (2022) 158396. https://doi.org/10.1016/j.scitotenv.2022.158396

[22] C. Wang, H. Lei, M. Qian, E. Huo, Y. Zhao, Q. Zhang, W. Mateo, X. Lin, X. Kong, R. Zou, R. Ruan, Application of highly stable biochar catalysts for efficient pyrolysis of

plastics: a readily accessible potential solution to a global waste crisis, Sustainable Energy Fuels 4 (2020) 4614-4624. https://doi.org/10.1039/D0SE00652A

[23] C. Wang, R. Zou, H. Lei, M. Qian, X. Lin, W. Mateo, L. Wang, X. Zhang, R. Ruan, Biochar-advanced thermocatalytic salvaging of the waste disposable mask with the production of hydrogen and mono-aromatic hydrocarbons, J. Hazard. Mater. 426 (2022) 128080. https://doi.org/10.1016/j.jhazmat.2021.128080

[24] C. Wang, H. Lei, X. Kong, R. Zou, M. Qian, Y. Zhao, W. Mateo, Catalytic upcycling of waste plastics over nanocellulose derived biochar catalyst for the coupling harvest of hydrogen and liquid fuels, Sci. Total Environ. 779 (2021) 146463. https://doi.org/10.1016/j.scitotenv.2021.146463

[25] K. Sun, N.J. Themelis, A.C. Bourtsalas, Q. Huang, Selective production of aromatics from waste plastic pyrolysis by using sewage sludge derived char catalyst, J. Clean. Prod. 268 (2020) 122038. https://doi.org/10.1016/j.jclepro.2020.122038

[26] X. Lin, H. Lei, E. Huo, M. Qian, W. Mateo, Q. Zhang, Y. Zhao, C. Wang, E. Villota, Enhancing jet fuel range hydrocarbons production from catalytic copyrolysis of Douglas fir and low-density polyethylene over bifunctional activated carbon catalysts. Energy Convers. Manag. 211 (2020) 112757. https://doi.org/10.1016/j.enconman.2020.112757

[27] A.A. Aboul-Enein, A.E. Awadallah, Production of nanostructure carbon materials via non-oxidative thermal degradation of real polypropylene waste plastic using La_2O_3 supported Ni and Ni-Cu catalysts, Polym. Degrad. Stab. 167 (2019) 157-169. https://doi.org/10.1016/j.polymdegradstab.2019.06.015

[28] A.A. Aboul-Enein, A.E. Awadallah, A novel design for mass production of multi-walled carbon nanotubes using Co-Mo/MgO catalyst via pyrolysis of polypropylene waste: effect of operating conditions, Fuller. Nanotub. Carbon Nanostructures 26 (2018) 591-605. https://doi.org/10.1080/1536383X.2018.1476344

[29] A.A. Aboul-Enein, A.E. Awadallah, Production of nanostructured carbon materials using Fe-Mo/MgO catalysts via mild catalytic pyrolysis of polyethylene waste, Chem. Eng. J. 354 (2018) 802-816. https://doi.org/10.1016/j.cej.2018.08.046

[30] D. Yao, C. Wu, H. Yang, Y. Zhang, M.A. Nahil, Y. Chen, P.T. Williams, H. Chen, Co-production of hydrogen and carbon nanotubes from catalytic pyrolysis of waste plastics on Ni-Fe bimetallic catalyst, Energy Convers. Manag. 148 (2017) 692–700. https://doi.org/10.1016/j.enconman.2017.06.012

[31] J. Gong, X. Chen, T. Tang, Recent progress in controlled carbonization of (waste) polymers, Prog. Polym. Sci. 94 (2019) 1–32. https://doi.org/10.1016/j.progpolymsci.2019.04.001

[32] S. Chen, Z. Liu, S. Jiang, H. Hou, Carbonization: A feasible route for reutilization of plastic wastes, Sci. Total Environ. 710 (2020) 136250. https://doi.org/10.1016/j.scitotenv.2019.136250

[33] M.R. Karimi Estahbanati, X.Y. Kong, A. Eslami, H.S. Soo, Current Developments in the Chemical Upcycling of Waste Plastics Using Alternative Energy Sources, ChemSusChem 14 (2021) 4152. https://doi.org/10.1002/cssc.202100874

[34] J. Wang, X. Li, M. Wang, T. Zhang, X. Chai, J. Lu, T. Wang, Y. Zhao, D. Ma, D, Electrocatalytic Valorization of Poly(ethyleneterephthalate) Plastic and CO_2 for Simultaneous Production of Formic Acid, ACS Catal. 12 (2022) 6722−6728. https://doi.org/10.1021/acscatal.2c01128

[35] H. Zhou, Y. Ren, Z. Li, M. Xu, Y. Wang, R. Ge, X. Kong, L. Zheng, H. Duan, Electrocatalytic upcycling of polyethylene terephthalate to commodity chemicals and H_2 fuel, Nat. Commu. 12 (2021) 4679. https://doi.org/10.1038/s41467-021-25048-x

[36] F. Ma, S. Wang, X. Gong, X. Liu, Z. Wang, P. Wang, Y. Liu, H. Cheng, Y. Dai, Z. Zheng, B. Huang, Highly efficient electrocatalytic hydrogen evolution coupled with upcycling of microplastics in seawater enabled via Ni_3N/W_5N_4 janus nanostructures, Appl. Catal. B: Environ. 307 (2022) 121198. https://doi.org/10.1016/j.apcatb.2022.121198

[37] R. Shi, K. S. Liu, F. Liu, X. Yang, C. C. Hou, Y. Chen, Electrocatalytic reforming of waste plastics into high value-added chemicals and hydrogen fuel, Chem. Commun. 57 (2021) 12595−12598. https://doi.org/10.1039/D1CC05032J

[38] T. Uekert, M. F. Kuehnel, D. W. Wakerley, E. Reisner, Plastic waste as a feedstock for solar-driven H_2 generation, Energy Environ. Sci. 11 (2018) 2853−2857. https://doi.org/10.1039/C8EE01408F

[39] T. Uekert, H. Kasap, E. Reisner, Photoreforming of Nonrecyclable Plastic Waste over a Carbon Nitride/Nickel Phosphide Catalyst, J. Am. Chem. Soc. 141 (2019) 15201−15210. https://doi.org/10.1021/jacs.9b06872

[40] M. Han, S. Zhu, C. Xia, B. Yang, Photocatalytic upcycling of poly(ethylene terephthalate) plastic to high-value chemicals, Appl. Catal. B: Environ. 316 (2022) 121662. https://doi.org/10.1016/j.apcatb.2022.121662

[41] C. Xing, G. Yu, J. Zhou, Q. Liu, T. Chen, H. Liu, X. Li, Solar energy-driven upcycling of plastic waste on direct Z-scheme heterostructure of V-substituted phosphomolybdic acid/g-C_3N_4 nanosheets, Appl. Catal. B: Environ. 315 (2022) 121496. https://doi.org/10.1016/j.apcatb.2022.121496

[42] J. Xu, X. Jiao, K. Zheng, W. Shao, S. Zhu, X. Li, J. Zhu, Y. Pan, Y. Sun, Y. Xie, Plastics-to-syngas photocatalysed by Co–Ga_2O_3 nanosheets, Natl. Sci. Rev. 9 (2022) nwac011. https://doi.org/10.1093/nsr/nwac011

[43] A.M. Al-Sabagh, F. Z. Yehia, D.R.K. Harding, Gh. Eshaq, A.E. ElMetwally, Fe_3O_4-boosted MWCNT as an efficient sustainable catalyst for PET glycolysis, Green Chem. 18 (2016) 3997-4003. https://doi.org/10.1039/C6GC00534A

[44] Y. Cha, Y.-J. Park, D.H. Kim, Hydrodynamic synthesis of Fe_2O_3@MoS_2 0D/ 2D-nanocomposite material and its application as a catalyst in the glycolysis of polyethylene terephthalate, RSC Adv. 11 (2021) 16841-16848. https://doi.org/10.1039/D1RA02335G

[45] M.R. Nabid, Y. Bide, M. Jafari, Boron nitride nanosheets decorated with Fe_3O_4 nanoparticles as a magnetic bifunctional catalyst for post-consumer PET wastes recycling, Polym. Degrad. Stab. 169 (2019) 108962. https://doi.org/10.1016/j.polymdegradstab.2019.108962

[46] I. Cano, C. Martin, J.A. Fernandes, R.W. Lodge, J. Dupont, F.A. Casado-Carmona, R. Lucena, S. Cardenas, V. Sans, I. de Pedro, Paramagnetic ionic liquid-coated SiO_2@Fe_3O_4 nanoparticles—The next generation of magnetically recoverable nanocatalysts applied in the glycolysis of PET, Appl. Catal. B: Environ. 260 (2020) 118110. https://doi.org/10.1016/j.apcatb.2019.118110

[47] T. Wang, C. Shen, G. Yu, X. Chen, Metal Ions Immobilized on Polymer Ionic Liquid as Novel Efficient and Facile Recycled Catalyst for Glycolysis of PET, Polym. Degrad. Stab. 194 (2021) 109751. https://doi.org/10.1016/j.polymdegradstab.2021.109751

[48] Q. Suo, J. Zi, Z. Bai, S. Qi, The Glycolysis of Poly(ethylene terephthalate) Promoted by Metal Organic Framework (MOF) Catalysts, Catal. Lett. 147 (2019) 240−252. https://doi.org/10.1007/s10562-016-1897-0

[49] T. Wang, C. Shen, G. Yu, X. Chen, The upcycling of polyethylene terephthalate using protic ionic liquids as catalyst, Polym. Degrad. Stab. 203 (2022) 110050. https://doi.org/10.1016/j.polymdegradstab.2022.110050

[50] C. Jehanno, I. Flores, A.P. Dove, A. Müller, F. Ruipérez, H. Sardon, Organocatalysed depolymerisation of PET in a fully sustainable cycle using thermally stable protic ionic salt, Green Chem. 20 (2018) 1205-1212. https://doi.org/10.1039/C7GC03396F

[51] C. Jehanno, J. Demarteau, D. Mantione, M.C. Arno, F. Ruiperez, J. L. Hedrick, A. P. Dove, H. Sardon, Synthesis of Functionalized Cyclic Carbonates through Commodity Polymer Upcycling, ACS Macro Lett. 9 (2020) 443–447. https://doi.org/10.1021/acsmacrolett.0c00164

[52] C. Jehanno, J. Demarteau, D. Mantione, M.C. Arno, F. Ruiperez, J. L. Hedrick, A. P. Dove, H. Sardon, Selective Chemical Upcycling of Mixed Plastics Guided by a Thermally Stable Organocatalyst, Angew. Chem., Int. Ed. 60 (2021) 6710−6717. https://doi.org/10.1002/anie.202014860

[53] C. Fan, L. Zhang, C. Zhu, X. J. Cao, Y. Xu, P. Sun, G. Zeng, W. Jiang, Q. Zhang, Efficient Glycolysis of PET Catalyzed by a Metal-Free Phosphazene Base: The Important Role of EG, Green Chem. 24 (2022) 1294−1301. https://doi.org/10.1039/D1GC03885K

[54] E. Nikolaivits, G. Taxeidis, C. Gkountela, S. Vouyiouka, V. Maslak, J. Nikodinovic-Runic, E. Topakas, A polyesterase from the Antarctic bacterium *Moraxella* sp. degrades highly crystalline synthetic polymers, J. Hazard. Mater. 434 (2022) 128900. https://doi.org/10.1016/j.jhazmat.2022.128900

[55] X. Xi, K. Ni, H. Hao, Y. Shang, B. Zhao, Z. Qian, Secretory expression in *Bacillus subtilis* and biochemical characterization of a highly thermostable polyethylene terephthalate hydrolase from bacterium HR29, Enzyme Microb. Technol. 143 (2021) 109715. https://doi.org/10.1016/j.enzmictec.2020.109715

[56] M. Hajighasemi, A. Tchigvintsev, B.P. Nocek, R. Flick, A. Popovic, T. Hai, A.N. Khusnutdinova, G. Brown, X. Xu, H. Cui, J. Anstett, T.N. Chernikova, T. Brüls, D. Le Paslier, M.M. Yakimov, A. Joachimiak, O.V. Golyshina, A. Savchenko, P.N. Golyshin, E.A. Edwards, A.F. Yakunin, Screening and characterization of novel polyesterases from environmental metagenomes with high hydrolytic activity against synthetic polyesters, Environ. Sci. Technol. 52 (2018) 12388–12401. https://doi.org/10.1021/acs.est.8b04252

[57] A. Bollinger, S. Thies, E. Knieps-Grünhagen, C. Gertzen, S. Kobus, A. Höppner, M. Ferrer, H. Gohlke, S.H.J. Smits., K.-E. Jaeger., A novel polyester hydrolase from the marine bacterium *pseudomonas aestusnigri* – structural and functional insights, Front. Microbiol. 11 (2020). https://doi.org/10.3389/fmicb.2020.00114

[58] V. Tournier, C. M. Topham, A. Gilles, B. David, C. Folgoas, E. Moya-Leclair, E. Kamionka, M. L. Desrousseaux, H. Texier, S. Gavalda, M. Cot, E. Guémard, M. Dalibey, J. Nomme, G. Cioci, S. Barbe, M. Chateau, I. André, S. Duquesne, A. Marty, An engineered PET depolymerase to break down and recycle plastic bottles, Nature 580 (2020) 216−219. https://doi.org/10.1038/s41586-020-2149-4

[59] C.-C. Chen, X. Han, X. Li, P. Jiang, D. Niu, L. Ma, W. Liu, S. Li, Y. Qu, H. Hu, J. Min, Y. Yang, L. Zhang, W. Zeng, J.-W. Huang, L. Dai, R.-T. Guo, General features to enhance enzymatic activity of poly(ethylene terephthalate) hydrolysis, Nat. Catal. 4 (2021) 425−430. https://doi.org/10.1038/s41929-021-00616-y

[60] H. Lu, D. J. Diaz, N. J. Czarnecki, C. Zhu, W. Kim, R. Shroff, D. J. Acosta, B. R. Alexander, H. O. Cole, Y. Zhang, N.A. Lynd, A.D. Ellington, H.S. Alper, Machine learning-aided engineering of hydrolases for PET depolymerization, Nature 604 (2022) 662−667. https://doi.org/10.1038/s41586-022-04599-z

[61] B. C. Knott, E. Erickson, M. D. Allen, J. E. Gado, R. Graham, F. L. Kearns, I. Pardo, E. Topuzlu, J. J. Anderson, H. P. Austin, G. Dominick, C.W. Johnson, N.A. Rorrer, C.J. Szostkiewicz, V. Copié, C.M. Payne, H. L. Woodcock, B.S. Donohoe, G.T. Beckham, J.E. McGeehan, Characterization and engineering of a two-enzyme system for plastics depolymerization, Proc. Natl. Acad. Sci. U.S.A. 117 (2020) 25476−25485. https://doi.org/10.1073/pnas.200675311

[62] A. Magnin, E. Pollet, R. Perrin, C. Ullmann, C. Persillon, V. Phalip, L. Avérous, Enzymatic recycling of thermoplastic polyurethanes: synergistic effect of an esterase and an amidase and recovery of building blocks, Waste Manage. 85 (2019) 141–150. https://doi.org/10.1016/j.wasman.2018.12.024

[63] J. Xin, Q. Zhang, J. Huang, R. Huang, Q.Z. Jaffery, D. Yan, Q. Zhou, J. Xu, X. Lu, Progress in the catalytic glycolysis of polyethylene terephthalate, J. Environ. Manage. 296 (2021) 113267. https://doi.org/10.1016/j.jenvman.2021.113267

[64] L. D. C. Bartolome, M. Imran, K. G. Lee, A. A. Sangalang, J. K. Ahn, D. H. Kim, Superparamagnetic γ-Fe_2O_3 nanoparticles as an easily recoverable catalyst for the chemical recycling of PET, Green Chem. 16 (2014) 279-286. https://doi.org/10.1039/C3GC41834K

[65] B. Zhu, D. Wang, N. Wei, Enzyme Discovery and Engineering for Sustainable Plastic Recycling, Trends Biotechnol. 40 (2022) 22-37. https://doi.org/10.1016/j.tibtech.2021.02.008

[66] H.Y. Sagong, H.F. Son, H. Seo, H. Hong, D. Lee, K.-J. Kim, Implications for the PET decomposition mechanism through similarity and dissimilarity between PETases from *Rhizobacter gummiphilus* and *Ideonella sakaiensis*, J. Hazard. Mater. 416 (2021) 126075. https://doi.org/10.1016/j.jhazmat.2021.126075

[67] Y. Cui, Y. Chen, X. Liu, S. Dong, Y.E. Tian, Y. Qiao, R. Mitra, J. Han, C. Li, X. Han, W. Liu, Q. Chen, W. Wei, X. Wang, W. Du, S. Tang, H. Xiang, H. Liu, Y. Liang, K.N. Houk, B. Wu, Computational Redesign of a PETase for Plastic Biodegradation under Ambient Condition by the GRAPE Strategy, ACS Catal. 11 (2021) 1340−1350. https://doi.org/10.1021/acscatal.0c05126

[68] H.F. Son, I.J. Cho, S. Joo, H. Seo, H.Y. Sagong, S.Y. Choi, S.Y. Lee, K.J. Kim, Rational Protein Engineering of Thermo-Stable PETase from *Ideonella sakaiensis* for Highly Efficient PET Degradation, ACS Catal. 9 (2019) 3519−3526. https://doi.org/10.1021/acscatal.9b00568

[69] M. Barth, A. Honak, T. Oeser, R. Wei, M.R. Belisário-Ferrari, J. Then, J. Schmidt, W. Zimmermann, A dual enzyme system composed of a polyester hydrolase and a carboxylesterase enhances the biocatalytic degradation of polyethylene terephthalate films, Biotechnol. J. 11 (2016) 1082–1087. https://doi.org/10.1002/biot.201600008

[70] W.L. Filho, A.L. Salvia, A. Bonoli, U.A. Saari, V. Voronova, M. Klõga, S.S. Kumbhar, K. Olszewski, D.M. De Quevedo, J. Barbir, An assessment of attitudes towards plastics and bioplastics in Europe, Sci. Total Environ. 755 (2021) 142732. https://doi.org/10.1016/j.scitotenv.2020.142732

[71] H. Wang, X. Liu, N. Wang, K. Zhang, F. Wang, S. Zhang, R. Wang, P. Zheng, M. Matsushita, Key factors influencing public awareness of household solid waste recycling in urban areas of China: A case study, Resour. Conserv. Recycl. 158 (2020) 104813. https://doi.org/10.1016/j.resconrec.2020.104813

946 **Figure captions**

947 **Fig. 1.** Global plastics use by polymers based on the data extracted from OECD Global
948 Plastics Outlook Database [1] (Note: HDPE, high-density polyethylene; LDPE, low-density
949 polyethylene; LLDPE, linear low-density polyethylene; PET, polyethylene terephthalate; PP,
950 polypropylene, PP&A fibers, polyphthalamide fibres; PS, polystyrene; PUR, polyurethane;
951 PVC, polyvinylchloride)

952 **Fig. 2.** Possible reaction mechanism for LDPE pyrolysis over biochar as acid catalyst

953 **Fig. 3.** Possible reaction pathways for the electrochemical oxidation of PET hydrolysate

954 **Fig. 4.** Possible reaction pathways for (a) the photo-reforming of polymer wastes (e.g., PET,
955 PLA) with alkaline pretreatment; (b) polymer wastes (e.g., polyethylene (PE)) without
956 alkaline pretreatment; (c) polymer wastes (e.g., polyethylene (PE)) without alkaline
957 pretreatment by VPOM/CNNS-15

958 **Fig. 5.** (a) Possible reaction pathways of glycolysis of PET using metal-based catalysts
959 (modified from Al-Sabagh et al. [43] and Bartolome et al. [64]); Note: M, metal ions; IL,
960 ionic liquid); (b) using protic ionic liquid (PIL) (Note, AN, anion of PIL; CA, cation of PIL;
961 Int. 1, intermediate 1; Int. 2, intermediate 2; Int. 3, intermediate 3)

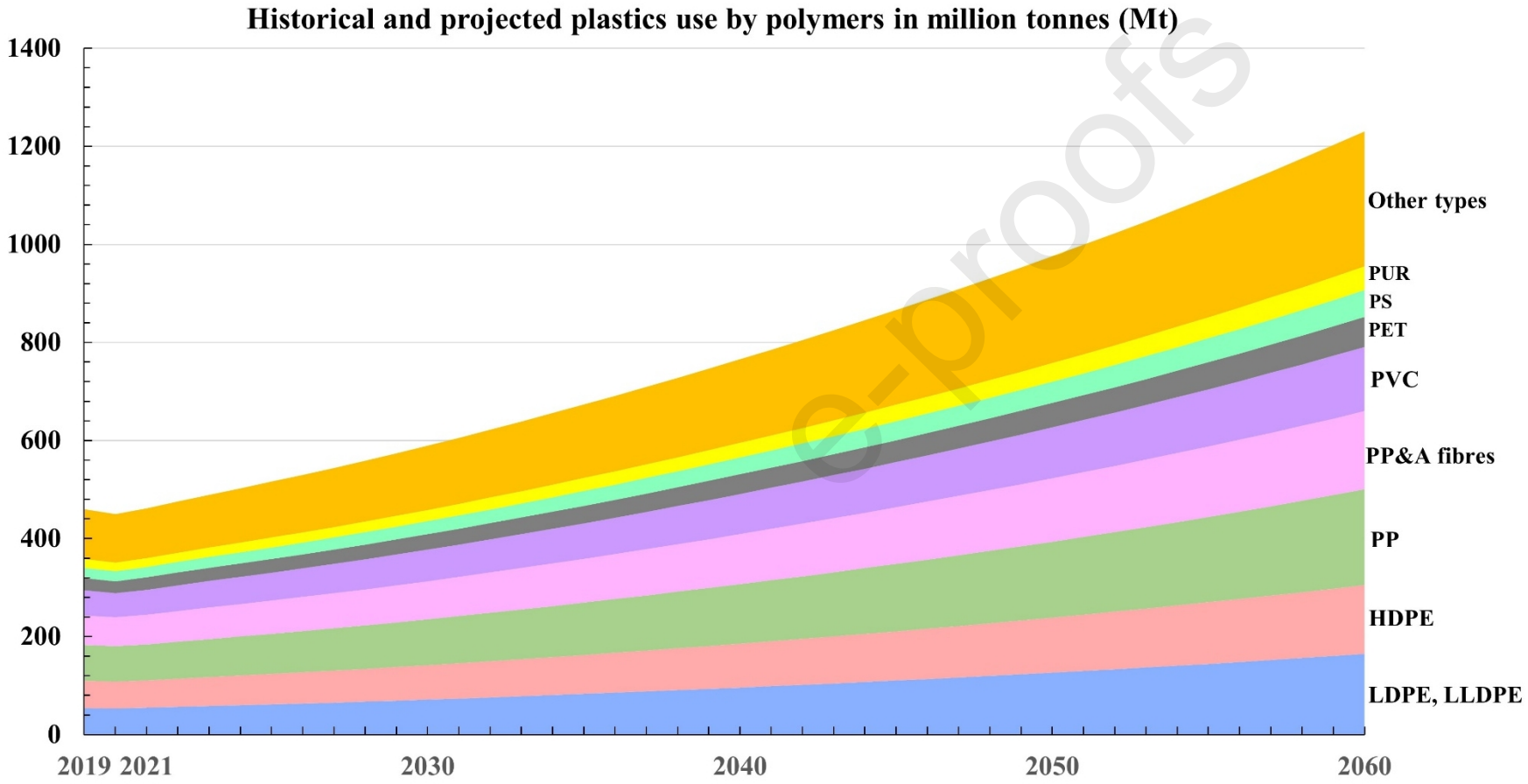

Fig. 1. Global plastics use by polymers based on the data extracted from OECD Global Plastics Outlook Database [1] (Note: HDPE, high-density polyethylene; LDPE, low-density polyethylene; LLDPE, linear low-density polyethylene; PET, polyethylene terephthalate; PP, polypropylene, PP&A fibres, polyphthalamide fibres; PS, polystyrene; PUR, polyurethane; PVC, polyvinylchloride)

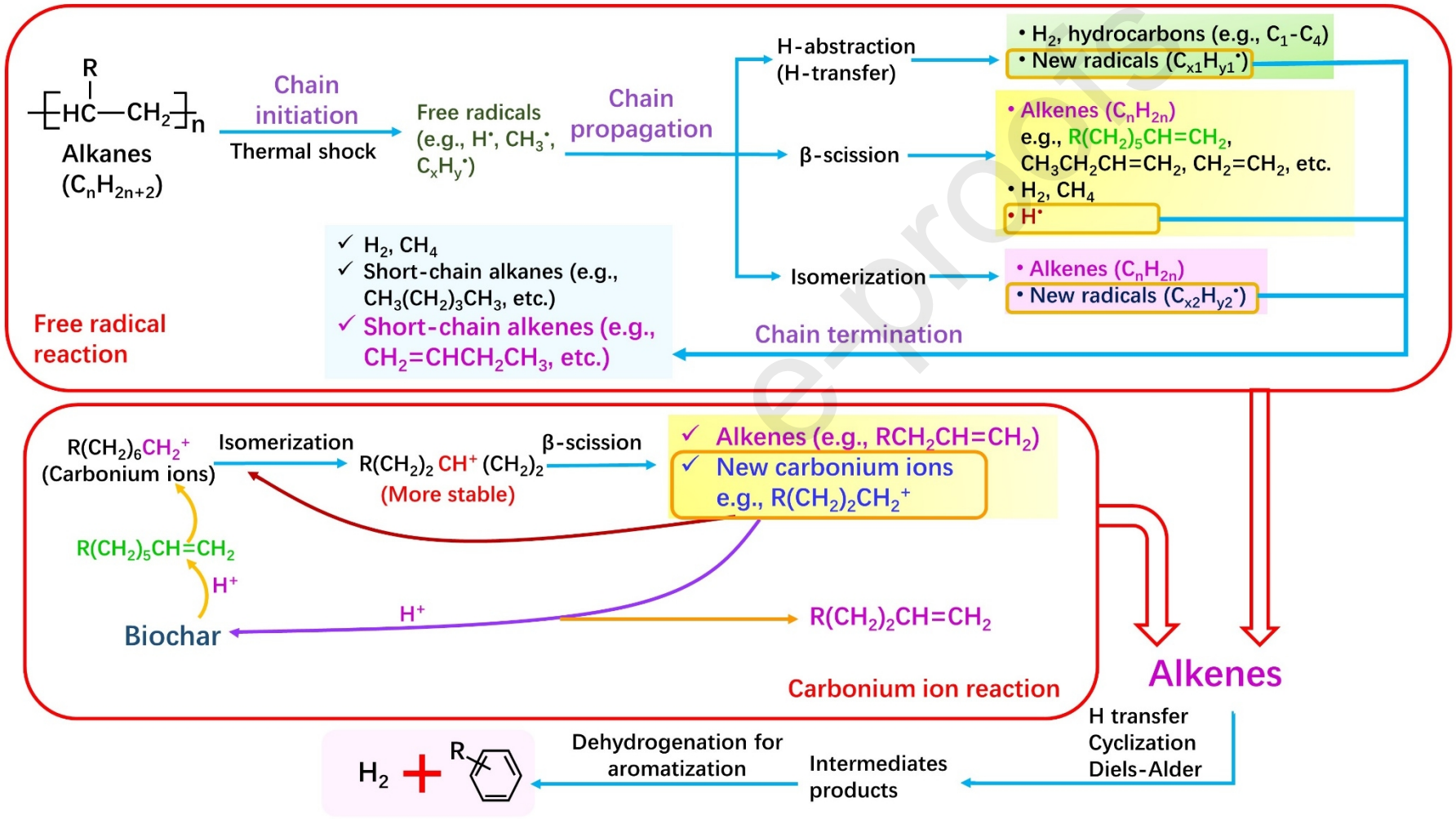

Fig. 2. Possible reaction mechanism for LDPE pyrolysis over biochar as acid catalyst

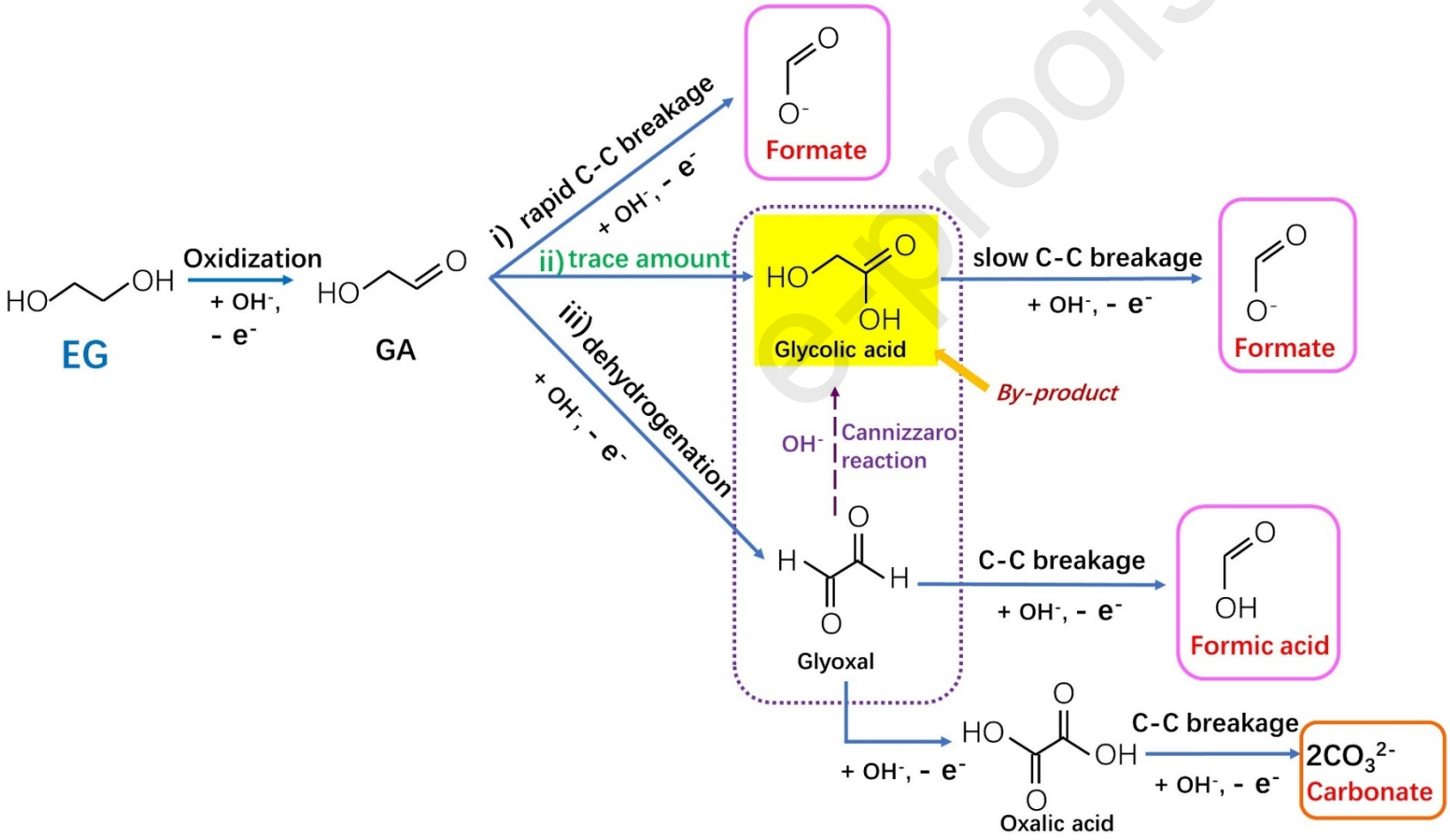

Fig. 3. Possible reaction pathways for the electrochemical oxidation of PET hydrolysate

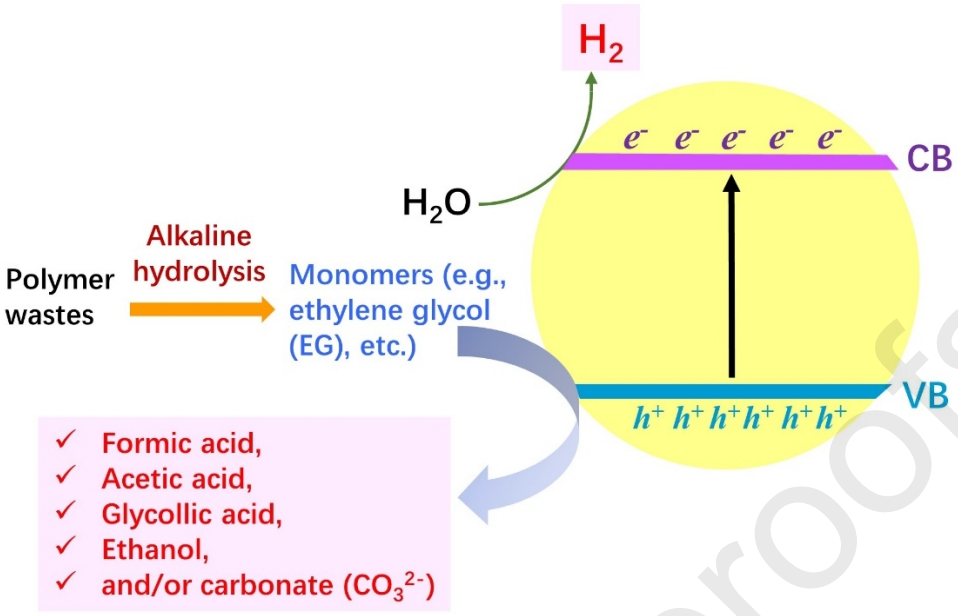
H2
H2O
e- e- e- e- e-
CB
VB
h+ h+ h+ h+ h+ h+
Polymer wastes
Alkaline hydrolysis
Monomers (e.g., ethylene glycol (EG), etc.)
✓ Formic acid,
✓ Acetic acid,
✓ Glycollic acid,
✓ Ethanol,
✓ and/or carbonate (CO3 2-)

(a)

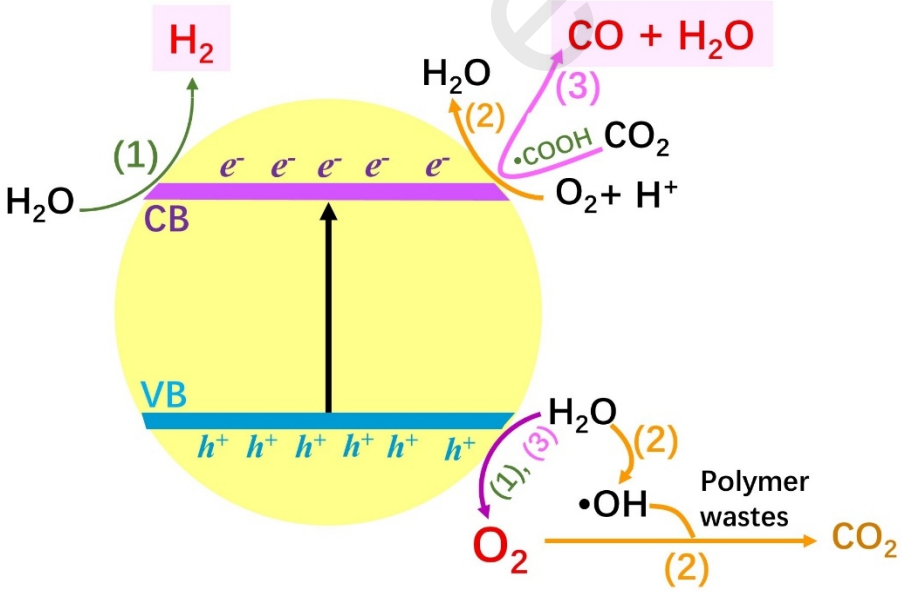
H2
CO + H2O
H2O
(1)
(2)
(3)
•COOH
CO2
O2+ H+
e- e- e- e- e-
CB
VB
h+ h+ h+ h+ h+ h+
H2O
(2)
(1), (3)
•OH
Polymer wastes
O2
CO2
(2)

(b)

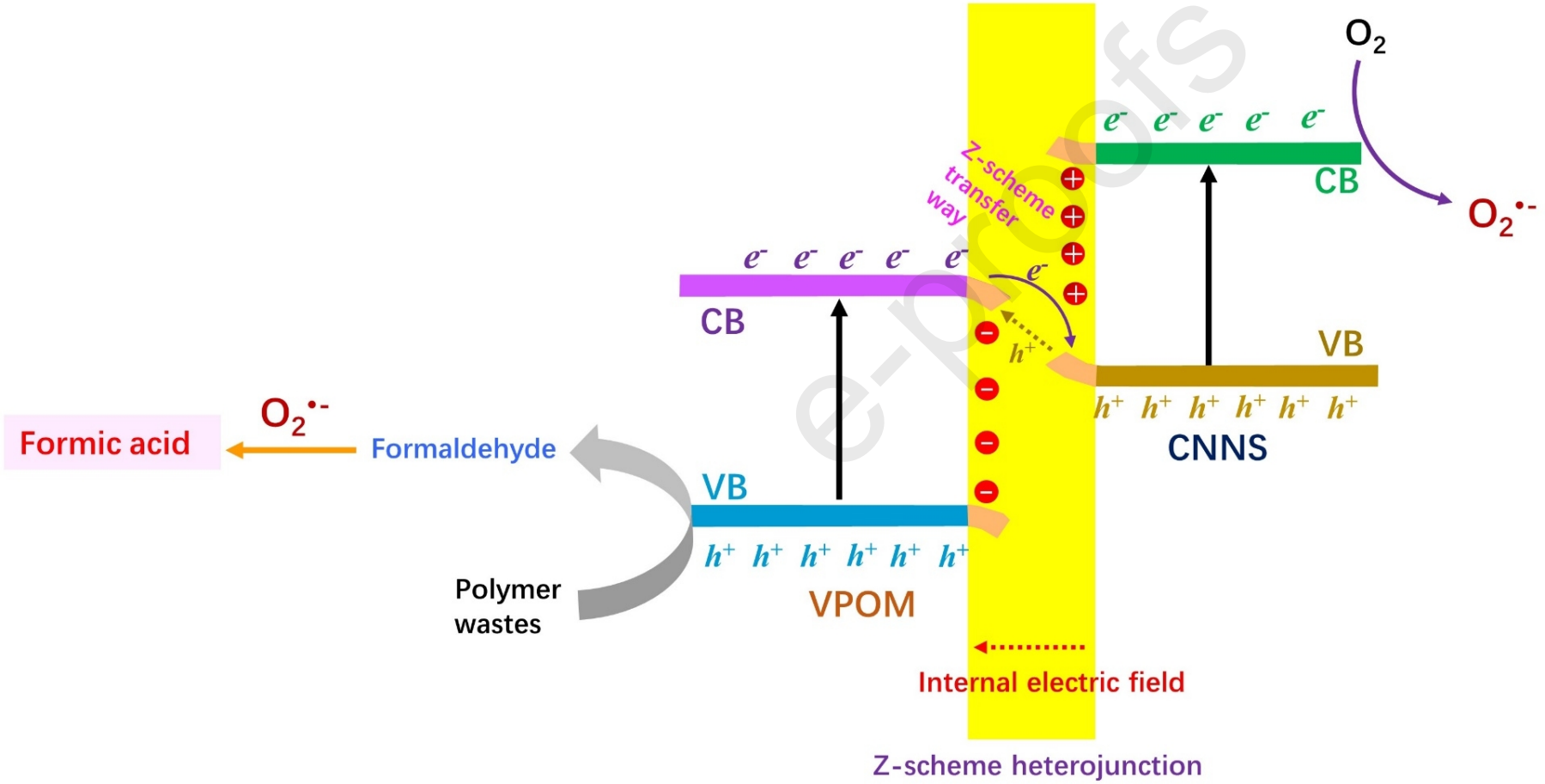

(c)

Fig. 4. Possible reaction pathways for (a) the photo-reforming of polymer wastes (e.g., PET, PLA) with alkaline pretreatment; (b) polymer wastes (e.g., polyethylene (PE)) without alkaline pretreatment; (c) polymer wastes (e.g., polyethylene (PE)) without alkaline pretreatment by VPOM/CNNS-15

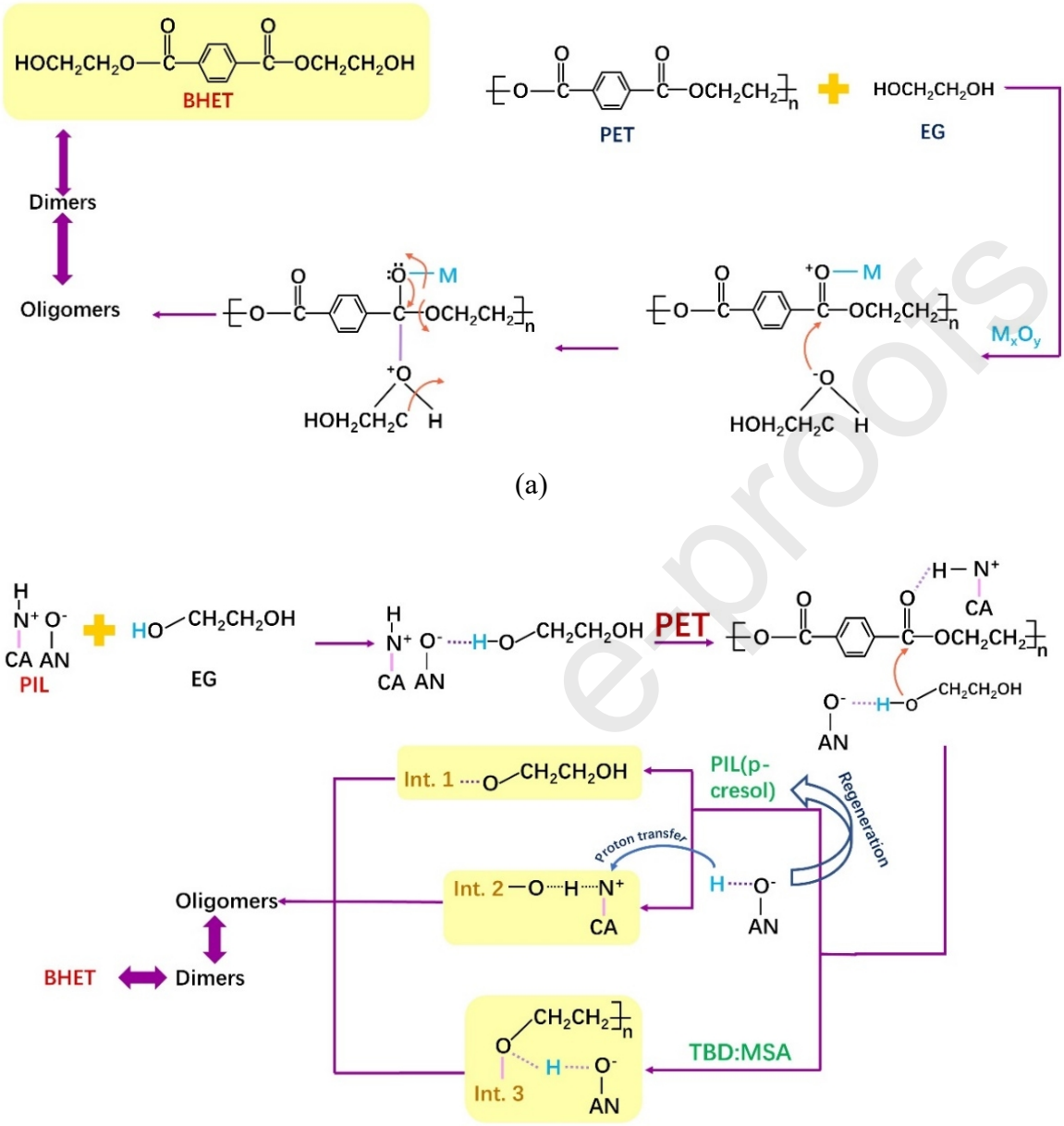

Fig. 5. (a) Possible reaction pathways of glycolysis of PET using metal-based catalysts (modified from Al-Sabagh et al. [43] and Bartolome et al. [64]; Note: M, metal ions; IL, ionic liquid); (b) using protic ionic liquid (PIL) (Note, AN, anion of PIL; CA, cation of PIL; Int. 1, intermediate 1; Int. 2, intermediate 2; Int. 3, intermediate 3)

Table titles

Table 1. Comparison of different catalytic upcycling approaches using common polymer wastes as feedstocks

Approaches	Polymer wastes	Cost[a]	Advantages	Disadvantages
Catalytic pyrolysis	HDPE, LDPE, PE, PP, PS, PVC, mixed plastics	R-L	✓ Simple process ✓ Being applicable for wide range of polymer wastes ✓ No need for complex pretreatment ✓ Being feasible for industrial applications	• Low selectivity and yield towards the specific product • High energy and temperature required • Need for product separation and upgrading
Carbonization	HDPE, LDPE, PE, PP, PS, PVC, mixed plastics	R-L	✓ Simple process ✓ Being applicable for wide range of polymer wastes ✓ Being able to maximize carbon formation by optimising pyrolysis and carbonization separately ✓ Controllable carbon products	• Higher temperature required than that for catalytic pyrolysis • High energy demand • Need for post-treatment (activation and surface modification) for product upgrading

			✓ Being feasible for industrial applications	
Electro-reforming	HDPE, PP, PE, PET	M	✓ A promising and sustainable approach ✓ Being powered by renewable electricity (solar, wind, and hydro) ✓ Being operated under mild conditions (ambient temperature and atmospheric pressure) ✓ Generation of electricity in an electrolytic cell ✓ Low energy demand for H_2 production	• Being at lab scale • Disposal of limited types of polymer wastes • Need for alkaline pretreatment • Slow oxidation rate
Photo-reforming	LDPE, PE, PET, PLA, PP, PS, PUR, PVC	L	✓ A sustainable and environmental-friendly way ✓ Being compatible with mixed polymer wastes ✓ Simple set-up	• Being at lab scale • Need for alkaline pretreatment • Low selectivity towards targeted products • Low yield of products

			✓ Being driven by clean and renewable solar energy ✓ Being operated under mild conditions (temperatures of 10-70 ºC and atmospheric pressure) ✓ Being able to scale up without adverse effects on the activity and performance	
Glycolysis	BPA-PC, PET, PUR	R-L	✓ Simple process ✓ Wide range of temperatures (130-225 ºC) ✓ Less volatile solvents ✓ Short reaction time ✓ Relatively high yield and selectivity towards BHET favourable for reproduction of PET ✓ Continuous production of targeted products	• Requirement of down-stream processes for product separation and purification • Complicated problems in optimising the trade-off between high yield of targeted products and total cost during practical operations (including catalysts and down-stream processes)

			✓ Being feasible for industrial applications	
Enzyme-assisted depolymerisation	PA, PBAT, PBSA, PCL, PET, PHAs, PHB, PLA, PUR	H	✓ An eco-friendly way ✓ Low energy demand ✓ Being compatible with mixed polymer wastes ✓ Being operated under mild conditions (25-72 ºC and atmospheric pressure) ✓ High chemoselectivity, regioselectivity, and stereoselectivity ✓ Being favourable for monomer recovery	• Being at lab scale • No disposal of polyolefins • Limited stability and activity of the enzyme • Misfolding and protein aggregation of the enzyme • Need for pretreatment to decrease crystallinity of polymer wastes

[a] R-L, relatively low cost; M, being cost-effective; L, low cost; H, high cost

Table 2. High-temperature conversion of polymers by catalysts

Approaches (Catalysts)	Feedstocks[a]	Temperature[b]	Value-added products[c]	By-products	References
Catalytic pyrolysis					
Biomass-derived biochar					
CSB (corn stover-derived biochar)	Model LDPE (catalyst/feedstock ratio = 3)	600 ºC	✓ Liquid product (40 wt% of total products) • 55-62% of C_8–C_{16} aliphatic hydrocarbons • 15-25% of mono-aromatic hydrocarbons • ~ 20% of C_{17}–C_{23} aliphatic hydrocarbons ✓ Gas yield (~ 60 wt% of total products): 60–80 vol% of H_2	Coke	[22, 24]
NCB (nanocellulose-derived biochar)			✓ Liquid product (38-40 wt% of total products) • 45-50% of C_8–C_{16} aliphatic hydrocarbons	Wax	

			• 42-46% of mono-aromatic hydrocarbons ✓ Gas yield (60-62 wt% of total products): 67-79 vol% of H_2		
NCB (nanocellulose-derived biochar)	Model LDPE (catalyst/feedstock ratio = 4)	500 ºC	✓ Liquid (~ 64 wt% of total products) • Mainly C_8–C_{16} aliphatic hydrocarbons and mono-aromatic hydrocarbons ✓ Gas yield (~ 36 wt% of total products): up to 92 vol% of H_2	/	[24]
CSB (corn stover-derived biochar)	Waste disposable mask (PP) (catalyst/feedstock ratio = 3)	600 °C	✓ Liquid (68-76 wt% of total products) • Mono-aromatics, especially toluene, xylenes, and ethylbenzene, ~63 wt% ✓ Gas yield (24-34 wt% of total products): ~ 55 vol% of H_2	/	[23]
NCB (nanocellulose-derived biochar)	Grocery bag (LDPE) (catalyst/feedstock ratio = 3)	600 ºC	✓ Liquid product (34 wt% of total products)	N.G.	[24]

		• 48.57% of C_8–C_{16} aliphatic hydrocarbons; • 42.05% of mono-aromatic hydrocarbons, • 9.37% of C_{17}–C_{23} aliphatic hydrocarbons	
		✓ Gas yield (66 wt% of total products): 77.55 vol% of H_2	
Grocery bag (HDPE) (catalyst/feedstock ratio = 3)		✓ Liquid product (33 wt% of total products) • 45.89% of C_8–C_{16} aliphatic hydrocarbons • 39.54% of mono-aromatic hydrocarbons • 7.56% of C_{17}–C_{23} aliphatic hydrocarbons • 5.29% of di-aromatics	N.G.
		✓ Gas yield (53 wt% of total products): 79.12 vol% of H_2	
Packaging trays (PP) (catalyst/feedstock ratio = 3)		✓ Liquid product (32 wt% of total products) • 17.13% of C_8–C_{16} aliphatic hydrocarbons;	N.G.

			• 77.77% of mono-aromatic hydrocarbons • 5.10% of di-aromatics ✓ Gas yield (68 wt% of total products): 69.82 vol% of H_2		
SSB (sewage sludge-derived biochar)	Mixed plastics (8 g; composition: 59 wt% PE, 22 wt% PP and 19 wt% PS) + catalyst (5 g)	600 ºC	✓ Monocyclic aromatics • Selectivity, 75.3% • Styrene in pyrolysis oil, up to 29.1% • Xylene in pyrolysis oil, up to12.5%	Coke	[25]
		800 ºC	✓ Bicyclic aromatics • Selectivity, up to 64.4% • Naphthalenes in pyrolysis oil, 47.5%	Coke	
10Fe/AC (corncob-derived biochar modified with Fe using $Fe(NO_3)_2$ solution at concentration of 10 wt%)	DF and LDPE (catalyst/feedstock ratio = 1)	500 ºC	✓ Bio-oil yield: 53.67% (mainly mono-aromatics) ✓ Gas yield (26.67% of total products): 44.32 vol% of H_2	Char and coke	[26]

Carbonization					
Metal-based catalysts					
NCL (bimetallic 40%Ni-10%Cu supported on La_2O_3)	PP (15 g) + catalyst (0.5 g)	700 ºC (DT)	✓ Carbon yield (51.9 wt% of total product): 1458% (maximum) • Mixture of large diameter full CNFs and MWCNTs with tubular structures ✓ Gas yield: 38.1 wt% of total product	Semi-solid or waxy hydrocarbons (yield, 10 wt% of total product)	[27]
Co-Mo/MgO (MgO supported Co-Mo catalyst containing 40 wt% of Co and 10 wt% of Mo)	PP (15 g) + catalyst (0.11 g)	800 ºC (DT)	✓ MWCNTs yield: 32.6 $g/g_{catalyst}$	N.G.	[28]
		850 ºC (DT)	✓ Mixture of GNSs and MWCNTs yield: 30. 6 $g/g_{catalyst}$		
$FeMo_{(0.8)}$/MgO (MgO supported Fe-Mo catalysts	LDPE (15 g) + catalyst (0.5 g)	750 ºC (DT)	✓ Carbon yield: 880 % (maximum) • GNSs/CNFs/CNTs hybrid materials, which contain few	N.G.	[29]

with Fe:Mo weight ratio of 40:10)			layers GNSs, large diameter CNFs and narrow diameter CNTs		
$FeMo_{(0.6)}$/MgO (MgO supported Fe-Mo catalysts with Fe:Mo weight ratio of 30:20)			✓ Carbon yield: 976 % (maximum) • GNSs/CNFs/CNTs hybrid materials with more stacked graphene sheets of GNSs than those generated over the $FeMo_{(0.8)}$/MgO	N.G.	
NiFe31/Al_2O_3 (bimetallic Ni-Fe catalysts prepared by dissolving $Ni(NO_3)_3$•$6H_2O$ and $Fe(NO_3)_3$•$9H_2O$ with Ni to Fe molar ratio of 3 in ethanol, and then adding Al_2O_3)	Mixed plastics (1 g; composition: 40 wt.% sample bottles (HDPE), 35 wt.% plastic bags (LDPE), 20 wt.% preservative boxes (PP) and 5 wt.% lunch boxes (PS)) + catalyst (0.5 g)	800 ºC (DT)	✓ Carbon yield: 46 g/100 g sample • Highly uniform and graphitized CNTs with narrow diameters, showing low carbon defect and high purity (yield:) ✓ H_2 yield: 7.24 g/100 g sample (content in gas product, 69.98 vol%)	N.G.	[30]

[a]DF, Douglas fir; LDPE, low-density polyethylene; HDPE, high-density polyethylene; PE, polyethylene; PP, polypropylene; PS, polystyrene

[b]DT, decomposition temperature

[c]CNTs, carbon nanotubes; CNFs, carbon nanofibers; GNSs, graphene nanosheets; MWCNTs, multi-walled carbon nanotubes

[d]N.G., not given

Table 3. Low- and intermediate-temperature depolymerisation of polymer wastes by catalysts

Approaches (Catalysts)	Feedstocks[a]	Temperature[b]	Value-added products[c]	By-products[d]	References
Electro-reforming					
Metal-based catalysts					
3D sponge-like Ni_3N/W_5N_4 Janus nanostructure	PET bottle (2.0 g of flasks)	AT	✓ Formic acid yield: 2.2 mmol at potential of 1.6 V for each cycle within 5 operational cycles (FE: ~ 85% at the potential range of 1.4-1.6 V) ✓ H_2	N.G.	[36]
Pd/NF-10 (being prepared by synthesizing palladium-modified nickel foam catalyst in 10 mM H_2PdCl_4)	PET (2.0 g)	AT	✓ PET conversion: almost 100% after 20 h ✓ Carbonate selectivity: 95% (FE: 93%) ✓ Terephthalate yield, up to 99%	N.G.	[37]

	Real-world plastic bottle (0.5 g)		✓ PET conversion: 100% after 25 h ✓ Carbonate selectivity: 95% (FE: 91%) ✓ Terephthalate yield: 96%; ✓ H_2 (FE: 98%)	N.G.	
$CoNi_{0.25}P$/NF (Co and Ni phosphides supported on nickel foam with feed atomic ratios of Ni/Co at 0.25)	Real-word PET (1 kg)	AT	✓ TPA yield: 818.5 g ✓ Formate yield: 389.2 g ✓ H_2 yield, 16.9 g	N.G.	[35]
$NiCo_2O_4$/CFP ($NiCo_2O_4$ grown on carbon fibre paper) as anode; SnO_2/CC (mesoporous SnO_2 electrocatalyst grown on carbon cloth) as cathode	PET (0.768 g of dried powder)	AT	✓ Formic acid (FE 155%, 85% at the anode and 70% at the cathode))	Trace amount of glycolic acid	[34]
Photo-reforming					

Metal-based catalysts					
CdS/CdO_x QDs (CdS/CdO_x quantum dots)	PLA (50 mg/L)	25 ºC	✓ H_2 yield: 0.511 ± 0.064 mmol H_2/g substrate after 4 h ✓ Pyruvate or an alkalinity-induced pyruvate-based compound	N.G.	[38]
	PET (25 mg/L)		✓ H_2 yield: 0.238 ± 0.039 mmol H_2/g substrate after 4 h ✓ Formate, glycolate, ethanol, acetate and lactate	N.G.	
	PUR (25 mg/L)		✓ H_2 yield: 0.053 ± 0.003 mmol H_2/g substrate after 4 h ✓ Formate, acetate, pyruvate and lactate	Aromatic component (e.g., 2,6-diaminotoluene)	
CN_x|Ni_2P (carbon nitride/nickel phosphide photocatalyst)	PET (25 mg/L)	25 ºC	✓ H_2 yield: 0.111 ± 0.008 mmol H_2/g substrate ✓ Carbonate, acetate, formate, glyoxal, glycolate, glyoxylate,	N.G.	[39]

			glycoaldehyde and ethanol		
	PLA (25 mg/L)		✓ H_2 yield: 0.211 ± 0.010 mmol H_2/g substrate ✓ Mainly carbonate and small quantities of acetaldehyde, pyruvate, formate and acetate	N.G.	
CPDs-CN-7 (carbonized polymer dots-graphitic carbon nitride composites with ratio of carbonized polymer dots to graphitic carbon nitride at 7:100 (w/w))	PET (1.25 g)	40 ºC	✓ H_2 yield: 2.8 mmol after 9 days (0.515 ± 0.168 mmol/g•h) ✓ Acetic acid, formic acid, acetaldehyde, glycolaldehyde, glycollic acid and ethanol	N.G.	[40]
	PLA (0.25 g)		✓ H_2 yield: 0.247 ± 0.038 mmol/g•h ✓ Carbonate	N.G.	
VPOM/CNNS-15 (a novel Z-scheme heterojunction prepared by assembling highly-dispersed phosphovanadomolybdates ($H_5PMo_{12-n}V_nO_{40}$, VPOM) clusters onto the surface of graphitic carbon nitride nanosheets	PE (20 mg)	20-40 ºC	✓ Formic acid yield: 0.0247 mmol/g•h (262 times higher compared with that of CNNS)	N.G.	[41]

(g-C_3N_4 nanosheets, CNNS) with ratio of VPOM to CNNS at 15:100 (w/w))					
Co–Ga_2O_3 nanosheets	Commercial PE bags (100 mg)	25 ºC	✓ H_2 yield: 0.648 mmol/g•h (~ 1.6 times higher than those of the Ga_2O_3 nanosheets) ✓ CO yield: 0.158 μmol/g•h (~ 1.9 times higher than those of the Ga_2O_3 nanosheets)	CO_2 yield: 0.419 mmol/g•h (~ 1.6 times higher than those of the Ga_2O_3 nanosheets)	[42]
Glycolysis					
Metal-based catalysts					
Fe_3O_4-boosted MWCNT (Fe_3O_4-boosted multiwalled carbon nanotubes)	PET (2 g)	190 ºC	✓ BHET yield: 100% after 8 cycles	N.G.	[43]
Fe_2O_3@MoS_2 0D/2D-nanocomposite material	Gf-PET (2 g of powder)	225 ºC	✓ BHET yield: 90% (> 80% after 7 cycles) ✓ PET conversion: 97%	Trace amount of Fe and Mo in BHET	[44]

				(0.0282 and 0.0018% w/w)	
Fe_3O_4 NPs@h-BNNS (a magnetic bifunctional catalyst by coating Fe_3O_4 nanoparticles on boron nitride nanosheets)	PET (0.3 g)	200 °C	✓ BHET yield: 100% (~ 90% after 4 cycles) ✓ BHET selectivity: 100%	N.G.	[45]
Fe_3O_4@SiO_2@(mim)[$FeCl_4$] (mim, methylimidazolium)	Gf-PET (100 mg)	180 °C	✓ BHET yield: ~ 84% over 12 cycles ✓ BHET selectivity: ~ 100% over 12 cycles	N.G.	[46]
Poly IL-Zn^{2+} (polymer [BVim]NTf2-metal ion (Zn^{2+}) complex precipitate; [BVim]NTf2, 1–butyl–3-vinylimidazolium bis[(trifluoromethyl)sulfonyl] imide)	PET (5 g)	195 °C	✓ BHET yield: 75.9% after 5 cycles ✓ PET conversion: 95.4%	N.G.	[47]
ZIF-8 (complex precipitate synthesized through mixing $Zn(NO_3)_2 \cdot 6H_2O$ and 2-methylimidazole (Hmim) in methanol and subsequently stirring at room temperature)	PET (5 g pellets)	197 °C	✓ BHET yield: > 70% after 3 cycles ✓ PET conversion: 100%	Oligomers and dimers	[48]

Glycolysis					
Organocatalysts					
PIL(p-cresol) (being prepared by mixing 1,5-diazabicyclo [4.3.0] -5-nonene (DBN) with 4-methylphenol)	PET (5 g)	190 °C	✓ PET conversion: 100% ✓ BHET yield: 87.3%	Dimers	[49]
TBD:MSA (an equimolar mixture of 1,5,7-triaza bicyclo[4.4.0]dec-5-ene (TBD) and methane sulfonic acid (MSA))	PET (0.5 g of flasks)	190 ºC	✓ PET conversion: 100% in less than 2 hours ✓ BHET yield: 90%	Dimers	[50]
TBD:MSA	BPA-PC (2 g of pellets)	130 °C	✓ BPA yield: 89% after 4 h ✓ Ethylene carbonate yield: 83% after 4 h	A derivative of a bis-carbonate of BPA attached with EG (yield, ~7%)	[51]
TBD:MSA	BPA-PC (2 g) + PET (1.5 g)	130 ºC	For selective depolymerisation of BPA-PC	A derivative of a bis-carbonate of BPA attached with EG (yield, 21% after 48 h)	[52]

			✓ BPA yield: 79% after 48 h (maximum 95% after 10 h) ✓ BHET yield: 7% after 48 h		
		180 °C	For full depolymerisation of PET ✓ BHET yield: 88% after 31 h ✓ BPA yield: 69% after 31 h (maximum 96% after 20 min with full depolymerization of BPA-PC)	A derivative of a bis-carbonate of BPA attached with EG (yield, ~ 40% after 48 h)	
t-BuP_2 (metal-free catalyst phosphazene base (Aladdin Bio-Chem Technology Co., Ltd (Shanghai, China))	PET (0.5 g)	190 °C	✓ BHET yield: 92.7% ✓ PET conversion: 100%	Oligomers	[53]
Enzyme-assisted depolymerisation					

Biocatalysts (enzymes)					
MoPE (the selected amino acid sequence from the Antarctic bacterium *Moraxella* sp. TA144)	PETa (10 mg/L; 0.66 mm thickness)	30 °C	✓ TPA	/	[54]
	Semi-crystalline PET powder (10 mg/L; 35% crystallinity, < 500 μm diameter)		✓ TPA + MHET yield: 1.3 μM ✓ TPA (~ 60% w/w of total products) ✓ MHET (~ 40% w/w of total products)	/	
	Amorphous PET powder (10 mg/L; ca 5% crystallinity)		✓ TPA (~ 60% w/w of total products) ✓ MHET (~ 40% w/w of total products) ✓ Obtaining 3.5-fold higher amounts of products compared to semi-crystalline PET powder ✓ Obtaining 6.6-fold higher amounts of products compared to amorphous film	/	

MoPE with FoFaeC (ratio of MoPE /FoFaeC of 2:1; FoFaeC, a feruloyl esterase)	Amorphous PET powder (10 mg/L; ca 5% crystallinity)		✓ TPA (DS to TPA: 1.5)	/	
	Semi-crystalline PET powder (10 mg/L; 35% crystallinity, < 500 μm diameter)		✓ TPA (DS to TPA: 1.4)	/	
*Bhr*PETase (A high-level secretory expression in *Bacillus subtilis* a PET hydrolase from the bacterium HR29)	PET powder (1% w/w in 100 mM HEPES buffer; 11.2% crystallinity)	70 °C	✓ TPA yield: 2.47 mM after 20 h ✓ MHET yield: 3.66 mM after 20 h ✓ BHET yield: 0.17 mM after 20 h	/	[55]
MGS0156	Solid PLA powder (10-12 mg)	30 °C	✓ Lactic acid monomers and oligomers (Conversion level: 95% overnight)	N.G.	[56]
GEN0105			✓ Lactic acid monomers and oligomers (Conversion level: ~ 70% overnight)	N.G.	

PE-H (a novel carboxylic ester hydrolase identified in the genome of the marine hydrocarbonoclastic bacterium *Pseudomonas aestusnigri* VGXO14^{T})	PETa, PETb	30 °C	✓ MHET yield: 4.2 ± 1.6 mg/L in 48 h	N.G.	[57]
PE-H (Y250S) (PE-H yielded variant obtained by introducing a single amino acid substitution (Y250S) into PE-H)			✓ MHET yield: 5.4 ± 0.6 mg/L in 48 h	N.G.	
ICCG (leaf-branch compost cutinase variant F243I/D238C/S283C/Y127G)	PcW-PET (200 g/kg of the total weight of the reaction volume (PET plus liquid phase) in Minibio bioreactors; 3 mg enzyme/g PET)	72 °C	✓ Depolymerisation level: 90% in 9.3 h ✓ TPA Productivity: 16.7 g_{TPA}/L•h after 24 h ✓ EG	N.G.	[58]
WCCG (leaf-branch compost cutinase variant F243W/D238C/S283C/Y127G)			✓ Depolymerisation level: 90% in 10.5 h ✓ TPA ✓ EG	N.G.	
*Bur*PL-DM (introducing double mutation of serine and isoleucine residues to *Is*PETase-like enzyme from *Burkholderiales* bacterium)	PET powder (5 mg)	35 ºC	✓ TPA + MHET yield: increase in the production of TPA + MHET by up to 3 times compared to that using *Bur*PL	N.G.	[59]

*Pb*PL-DM (introducing double mutation of serine and isoleucine residues to *Is*PETase-like enzyme from *Polyangium brachysporum*)	40 ºC	✓ TPA + MHET yield: increase in the production of TPA + MHET by around 10 times compared to that using *Pb*PL	N.G.
*Ct*PL-DM (introducing double mutation of serine and isoleucine residues to *Is*PETase-like enzyme from *Caldimonas taiwanensis*)	60 ºC	✓ TPA yield: 6.74±1.21 µM vs < 2 µM using *Ct*PL ✓ MHET yield: 23.12±2.14 µM vs < 2 µM using *Ct*PL	N.G.
PET2-DM (introducing double mutation of serine and isoleucine residues to the enzyme obtained from uncultured bacterium (type IIa enzyme))	50 ºC	✓ TPA yield: 30.31 ± 0.13 µM vs 8.47 ± 0.31µM using PET2 ✓ MHET yield: 5.31 ± 0.13 µM vs 12.84 ± 1.44 µM using PET2	N.G.
*Tf*Cut-DM (introducing double mutation of serine and isoleucine residues to cutinases from *Thermobifida fusca*)	60 ºC	✓ TPA + MHET yield: > twofold increment in production of MHET and TPA compared to *Tf*Cut	N.G.

FAST-PETase (PETase$^{S121E/D186H/R224Q/N233K/R280A}$ as the functional, active, stable and tolerant PETase)	Circular Gf-PET film (11.4 mg)	50 °C	✓ PET monomers (TPA+MHET yield: 33.8 mM in 96 h)	N.G.	[60]
	Hole-punched films from pretreated PET(MRQ) water bottle (25 mg; crystallinity, ~ 2%)		✓ PET monomers (TPA+MHET yield: 32.8 mM in 24 h)	N.G.	
	Hole-punched films from pretreated PET(MQ) water bottle (25 mg; crystallinity, 23.6%)		✓ PET monomers (TPA+MHET yield: 23.8 mM in 24 h)	N.G.	
	Complete and non-physically disrupted melted plastic puck from an entire PET water bottle (~ 9 g)		✓ PET monomers (TPA+MHET yield: >200 mM in 14 days for complete degradation)	N.G.	

	Large, untreated, and green coloured pc-PET flasks (3.0 g)		✓ Complete degradation of the coloured pc-PET flasks after 6 days ✓ PET monomers including TPA and MHET ✓ TPA yield: 4.3 g (recovery of 94.9% from degradation solution, purity of over 97%)	N.G.	
Ideonella sakaiensis PETase plus MHETase	Amorphous Gf-PET film (crystallinity, 2-3%; 0.1-2 mg PETase/gPET, 0.1-1 mg MHETase/gPET)	30 ºC	✓ TPA yield: 0.12 ± 0.03 mM~2.87 ± 0.13 mM	/	[61]
Amidase (E4143) + esterase (E3576)	TPU (pieces, 50-80 mg)	37 °C	✓ 6-hydroxycaproic acid yield: ~ 1 g/L ✓ MDA and MDA linked to a caprolactone unit yield: 0.3-3 mg/L	Potential inhibitor with a urethane bond	[62]

[a]BPA-PC, bisphenol A-based polycarbonate; Gf-PET film, Goodfellow PET film; Pretreated PET(MQ) water bottle, being obtained through melting and directly temperature quenching; Pretreated PET(MRQ) water bottle, being obtained through melting, reheating and subsequently quick temperature quenching; PcW-PET, post-consumer

coloured-flake PET waste; PE, polyethylene; PET, polyethylene terephthalate; PETa, amorphous PET film; PETb, PET from a commercial single use bottle; PLA, polylactic acid; PUR, polyurethane; TPU, thermoplastic polyurethanes

[b]AT, Ambient temperature

[c]BHET, bis(2-hydroxyethyl) terephthalate; BPA, bisphenol A; DS, the degree of synergism; EG, ethylene glycol; FE, Faradic efficiency; MDA, 4,4'-methylene dianiline; MHET, mono(hydroxyethyl) terephthalate; TPA, terephthalic acid

[d] N.G., not give